Review Article

Muhamad Imam Firdaus* and Ristiyanto Adiputra*

Deterioration and imperfection of the ship structural components and its effects on the structural integrity: A review

https://doi.org/10.1515/cls-2024-0008
received December 31, 2023; accepted April 11, 2024

Abstract: The design of ship structural safety is crucial to ensure the ship's survivability during the operation. Extensive research has been conducted on ship structural components, including box girders, stiffened panels, and plates, beyond the ideal conditions by considering the implication of manufacturing processes, vessel usage, and aging in the form of defects like cracks, corrosion, and imperfections, both locally and globally. Previous research has also explored various methodologies, conditions, and parameters to understand the impact of damages and imperfections on ship structure and strength. However, there is a significant need to bridge the gap in prior research to advance technology and ship structural strength analysis. A comprehensive benchmark study specifically focused on improving ship structural component needs, identifying differences and gaps among existing studies as challenging. This article thoroughly reviews ship structural components, such as box girders, stiffened panels, and plates, while examining the effects of structural defects like corrosion, cracks, and imperfections on ship structural integrity. It synthesizes the influence of various defect parameters, including crack length, angle, position, corrosion severity, pit corrosion, pit diameter, and pit models, using finite element modeling and experimental investigations, particularly emphasizing ship structural components. The comparative analysis of methods and parameters presented in this review will serve as a valuable reference for future investigations and studies related to ship structural strength and design. The article's contribution is expected to enhance the understanding of ship structural strength, contributing to the sustainability and effectiveness of vessel design in the global maritime industry.

Keywords: stiffened plate, stiffened panel, box girder, ultimate strength, structural imperfection

Nomenclature

$2c/b$	Ratio between crack length and section width
A_{0i}	Amplitude of hungry horse imperfection mode
A_1, A_j	Amplitude of ARE imperfection mode
A_B	The total sectional area of the outer bottom
A'_B	The total sectional area in the inner bottom
A_D	The total sectional area of the deck
A_{j+1}	High-order amplitude of ARE imperfection mode
A_s	The total sectional area of the side shell
a	Span length
B_0	Amplitude of torsional and column imperfection mode
b	Plate width
b_1	The breadth of the longitudinal tensile residual stress block
C_0	Amplitude of local imperfection mode
D	The hull depth
E	Modulus young
g	The neutral axis position above the baseline
H	The depth of the hull section of the linear elastic state
hs	The maximum height of the web
j	Half-wave number of the buckling mode
L_w	Weld leg length
M_u	Ultimate bending moment
m	Half-wave number of the buckling mode
Rf	Ratio between cracked ultimate strength of box girder and ultimate strength of box girder in initial condition
t	Plate thickness
v	Ratio Poisson

*** Corresponding author: Muhamad Imam Firdaus,** Surabaya Merchant Marine Polytechnic, Surabaya, 12760, Indonesia, e-mail: imam.firdaus@poltekpel-sby.ac.id
*** Corresponding author: Ristiyanto Adiputra,** Research Center for Hydrodynamics Technology, National Research and Innovation Agency (BRIN), Surabaya, 60112, Indonesia, e-mail: ristiyanto.adiputra@brin.go.id

W_c	Column imperfection mode
W_l	Local plate imperfection mode
W_t	Torsional imperfection mode
w_{opl}	Plate distortion
w_{opl}^{max}	Maximum magnitude of plate distortion
x	Coordinate
x_i	Coordinate
y	Coordinate
y_i	Coordinate
z	Elastic section modulus
z_i	Coordinate
β	Plate slenderness
ε	Strain
ε_y	Yield strain
ε_{rcx}	Compressive residual strain
ε_Y	Compressive yield strain
η	Constant
θ	Angle
λ	Column slenderness
λ_τ	The ratio between the shear and longitudinal in-plane stresses
σ	Strength
σ_0	The magnitude of residual compression stress
σ_{cr}	Critical bending stress
σ_E	Bending stress
σ_r	The magnitude of residual tensile stress
σ_u	Ultimate strength
σ_{uD}	The ultimate buckling strength for deck
σ_{uS}	The ultimate buckling strength for side
σ_x	Longitudinal stress
σ_{xu}	Ultimate strength of corroded plates
σ_{xu0}	Ultimate strength of initial plates
σ_y	Yield stress
σ_{y1}	Transversal stress
σ_{yB}	The yield strength outer bottom
σ'_{yB}	The yield strength Inner bottom
σ_{yS}	The yield strength side
ϕ	Edge function

1 Introduction

The safety and structural integrity of ships are paramount in ensuring secure transportation. Modes of maritime transportation such as bulk carriers, oil tankers, and very large crude carriers (VLCCs) require special attention due to their crucial role in distributing raw materials. Bulk carriers transport commodities such as cement, grains, coal, and oil, while oil tankers play a vital role in the sea-based distribution of crude oil products [1,2]. Both bulk carrier vessels transporting raw materials and passenger ships such as Ro–Ro ships are susceptible to structural failure due to grounding, collisions with other vessels, or fatigue resulting from continuous loading over a certain period [3–7]. Numerous accidents involving these vessels have resulted in environmental damage, as highlighted by Brubaker [8], who estimated that between 600,000 and 1.8 million tons of oil spills routinely pollute the seas each year. This unfortunate situation is unavoidable due to the recurring accidents that plague these vessels annually.

Ship accidents resulting from structural failures were quite common, with records showing significant incidents involving bulk carriers from the 1970s to the 1990s [9,10]. The number of such accidents has continued to rise, as indicated by a study conducted by Eliopoulou, which documented a total of 146 accidents caused by structural failure involving various types of oil tankers, ranging from VLCCs to ultra-large crude carriers, from 1990 to 2020. It is worth emphasizing that ship accidents caused by structural failure have historically contributed significantly to maritime accidents, even in the past two decades. As key players in the global economy, addressing this issue is essential, considering its far-reaching impacts, including loss of life, property damage, and broader concerns such as marine and coastal environmental pollution [11].

Through the common structural rules (CSR), safety and regulations regarding ship design are governed by the ultimate limit state (ULS) parameter. Various approaches have been conducted to enhance the ship strength, including experimental, analytical, and numerical studies. In 2020, The International Association of Classification Societies (IACS) released IACS-CSR in Part III.1, which focuses on ultimate strength, compiles findings from researchers, and investigates recent developments in ship research. The widespread technological advancements have enabled us to analyze the ship strength not only through experimental methods but also through numerical methods using various commercial software. The utilization of these methods has led to innovations such as the development of formulas for calculating strength, as demonstrated in the studies conducted by Kim *et al.* [12] and Xu *et al.* [13], who used plate slenderness functions to determine the ultimate strength of stiffened panels. This extends beyond stiffened panels, as research on simpler structures like plates and more complex ones like box girders has also been extensively conducted.

The development of ship safety and structural strength is achieved by incorporating the aspect of initial imperfection. In actual conditions, initial imperfections occur due to factors such as the influence of fabrication processes like welding, damage from usage, and age-related wear and tear. Effects such as residual stress in the structure due

to welding processes are addressed by reducing the yield stress value or decreasing the plate and stiffener thickness due to corrosion effects. These improvisations have been integrated into ship strength analysis. Investigations and studies conducted on cases involving the introduction of initial imperfections have yielded accurate results that match real-world conditions. Therefore, this consideration is being evaluated for adoption as a standard in the IACS-CSR with adjustment through a correction factor.

The advent of technological advancements, such as numerical analysis, provides a more efficient solution for predicting ship strength. However, there is a need for validation between modeling parameters and experimental analysis to ensure that the results align with real-world conditions. The development of numerical analysis has given rise to various approaches to defining simulation parameters, prompting [14] to compare different types of boundary conditions, namely, symmetric and periodic boundary conditions. The findings revealed a significant deviation between the two under certain conditions and minor deviations under specific circumstances. Another parametric study was conducted by Hanif *et al.* [15], focusing on the configuration area and the modeling of transverse stiffeners. Adiputra *et al.* [16] utilized numerical calculations to predict ship operational times under hogging and sagging conditions, considering various factors such as geometry and initial imperfections. More recently, in larger ship structures, Denev [17] conducted research and found that waste corrosion can affect the section modulus and ultimate strength.

In this present article, a review of significant literature related to the research advancements in ship structural strength through various methods, including experiments, analytics, and numerical analyses using various software, was conducted. Various influences and factors, such as the type, size, and distribution of initial imperfections on plates, stiffened panels, and box girders are also discussed to understand the postbuckling behavior of each variation. In addition, differences in approaches to numerical studies are explored to provide insights into future research trends in this field.

2 Plate

The strength of a ship's plate structure significantly influences the overall strength of the ship's structure. A ship's structure can be regarded as a combination of reinforced plates seamlessly joined with approximately equal spacing between each other [18]. Plates themselves constitute the primary structural components in ship structures. Since plate elements typically form a larger amalgamation known as stiffened plates, any failure occurring within the stiffened plate will only happen when all plates experience failure simultaneously [19]. Therefore, the upper limit of failure due to plates is the summation of the maximum load-bearing capacity of all plate elements while also taking into account the role of stiffeners.

2.1 Ultimate strength of stiffened plate

The design of ship structures can be considered as rectangular boxes enveloped by stiffened panels. A clearer depiction of the ship's structure can be observed in Figure 1. Subsequent research in ship structure design emphasizes buckling conditions and the ultimate strength of the ship's structure. The ultimate strength of a structure or system is defined as a point where the incremental addition of applied loads cannot be sustained or supported by the structure so that when it surpasses the ultimate point, the structure experiences failure and collapse. An illustration of ultimate strength is presented in Figure 2.

Buckling and the ultimate strength of plates themselves are fundamentally crucial for the strength of a ship, both locally and globally. In this regard, the plate slenderness ratio is a critical parameter. Plate slenderness can be defined by the following equation:

$$\beta = (b/t)\sqrt{\sigma_y/E}\,, \tag{1}$$

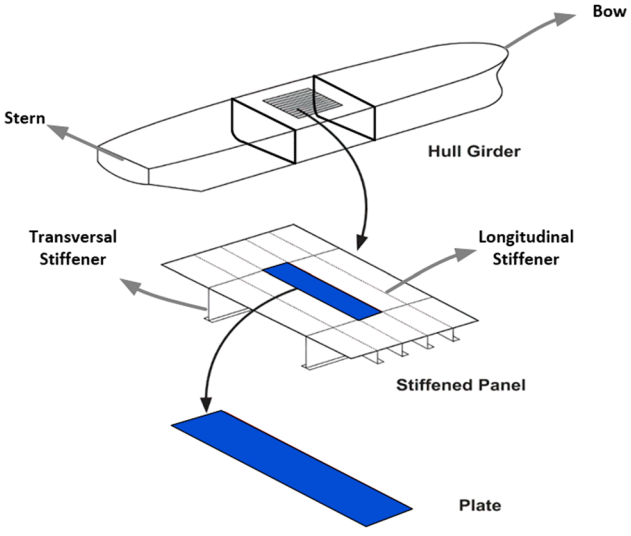

Figure 1: Illustration of ship structure produced based on the information obtained from the study by Zhang [20].

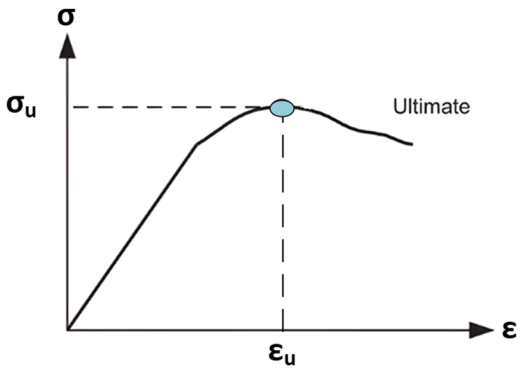

Figure 2: Ultimate strength point illustration. Produced based on the information obtained from the study by Zhang [20].

where σ_y represents the yield stress, E is the Young's Modulus of the material employed, and t denotes the plate thickness.

Further research on the structural design of modern oil tankers and bulk carriers with lengths ranging from 150 to 400 m indicates that the ratio of plating, denoted as a/b, between stiffeners and transverse frame ranges from 3.5 to 6.7 in both the deck and bottom sections of the mid-ship. The ratio of width to thickness of plating, represented as b/t, falls within the range of 25–65. The plate thickness ranges from 12 to 26 mm. The area of the plate itself accounts for approximately 60–80% of the cross-sectional area of the stiffened panel [20].

In ship plate structures, the most common loading scenario typically involves a combination of longitudinal loads, transverse loads, shear loads, and lateral loads [18]. Several studies have conducted strength analyses of ship plates under both combined and single loads, with the primary loading component on the deck structure and the bottom structure being axial compressive loads. Therefore, in standard design analysis of the entire hull girder, the main loading component considered is the longitudinal load. However, the bottom plating and the lower portion of the side shell can also be subjected to relatively high additional loads from lateral pressure. Furthermore, the inner bottom and inner longitudinal bulkhead can experience pressure loads from cargo loads. This lateral pressure, whether directly applied or through hull frame bending, generates transverse loads within the plate plane.

Due to the crucial and intricate nature of ultimate strength and buckling in plate structures, this field has been studied and researched for over 100 years. Further research into the analysis of ultimate strength in the plate structures is primarily conducted using axial compression loads, with various enhancements and updates in terms of analysis methods and geometric variations. In the axial loading analysis, the model considered is a simple, longitudinally supported plate subjected to axial forces, as depicted in Figure 3.

In the initial loading stage, the plate experiences axial compressive forces and behaves linearly. Subsequently, as additional loads are applied, lateral deflection increases, and simultaneously, minor yielding occurs on the long side of the plate. This results in the load-shortening curve becoming nonlinear. Structural failure occurs when the ultimate state is reached, followed by significant lateral deflection and failure near the long side [20]. Examples of load-shortening curves for plates with thicknesses of 32, 18, and 12 mm can be seen in Figure 4.

The classic equation regarding elastic buckling stress for plates can be observed in Eq. (2):

$$\frac{\sigma_E}{\sigma_y} = \frac{\pi^2 E}{3(1-\nu^2)}\left(\frac{b}{t}\right)^2 \approx \frac{3.62}{\beta^2}. \tag{2}$$

However, using the aforementioned equation and the compression analysis method explained earlier, accurate results cannot be obtained for certain plate thicknesses. For instance, when $\beta = 1$, the buckling stress will be 3.6 times the yield stress, resulting in inaccurate outcomes. Therefore, an equation based on empirical corrections for critical buckling at specific plate thicknesses is subsequently adopted, as depicted in Eq. (3):

$$\frac{\sigma_{cr}}{\sigma_y} = 1 - \frac{1}{4}\frac{\sigma_y}{\sigma_E}, \text{ for } \frac{\sigma_y}{\sigma_E} > \frac{1}{2}. \tag{3}$$

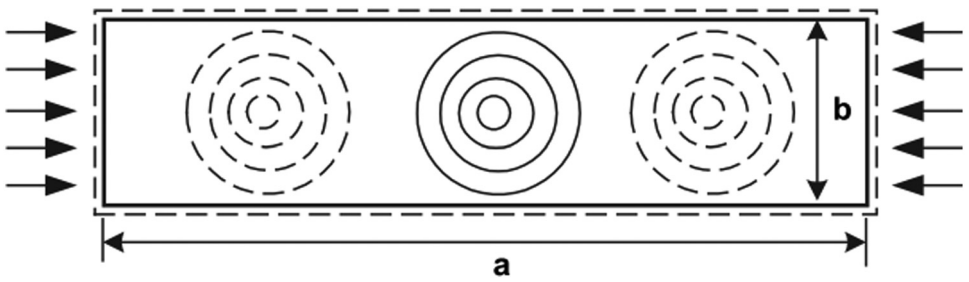

Figure 3: Example of loading set up on plate analysis [21].

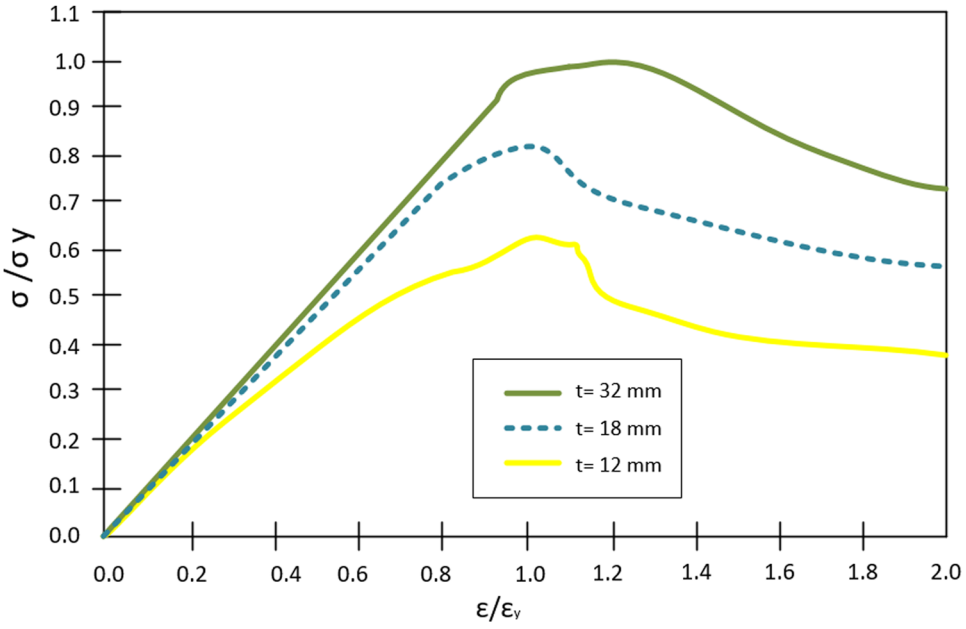

Figure 4: Examples of load-shortening curves at different plate thicknesses illustrated based on the information obtained from the study by Zhang [20].

In the evolution of scientific knowledge in the field of plate strength analysis, the initial research on ultimate strength and the formulation of plate strength equations were conducted by Box in 1883, followed by further studies carried out by von Karman in 1924. During the period from 1883 to 1975, several formulas for analyzing plate ultimate strength were proposed, mainly through semi-analytical and empirical approaches. Some of these can be seen in Eqs. (4) and (5).

Box [22]:

$$\frac{\sigma_u}{\sigma_y} = \frac{1}{\beta^{0.5}}. \tag{4}$$

Von karmam [23]:

$$\frac{\sigma_u}{\sigma_y} = \frac{1.9}{\beta}. \tag{5}$$

Schnadel [24]:

$$\frac{\sigma_u}{\sigma_y} = 0.5 + \frac{1.81}{\beta^2}. \tag{6}$$

Frankland [25]:

$$\frac{\sigma_u}{\sigma_y} = \frac{2.25}{\beta} - \frac{1.25}{\beta^2}. \tag{7}$$

Faulkner [26]:

$$\frac{\sigma_u}{\sigma_y} = \frac{2}{\beta} - \frac{1}{\beta^2}. \tag{8}$$

Widely adopted formulas for calculating the ultimate strength of plates under axial compression, such as the Frankland and Faulkner equations, required significant development time due to their inherently complex parameters. Both of these formulas, despite some differences, have become standard equations utilized. Many researchers have subsequently proposed alternative equations for calculating the ultimate strength of plates, as suggested by Paik and Pedersen [27].

One of the studies on the analysis of plates under axial compression was conducted by Zhang and Khan [21]. The research was performed using Faulkner's equation and then compared with nonlinear finite element analysis (FEA). In the nonlinear FEA, a simple supported plate model with a length (a) of 4,300 mm and width (b) of 815 mm was used. This plate was referenced from a double-hull oil tanker with a length of 230 m. A parametric study was conducted with plate thickness ranging from 11.8 to 32 mm, equivalent to β values ranging from 1 to 2.7. The plate was assumed to have five and a half waves in the longitudinal direction and one and a half waves in the transverse direction. The results of the comparison between FEA and calculations using Faulkner's equation showed that the FEA results aligned with

Faulkner's equation calculations. The difference between the two was less than 0.5% for β values between 1.5 and 2.5, demonstrating the reliability of the FEA.

2.2 Analysis of plate with cracks

Subsequently, research on plates was extended to include the introduction of cracks in plate structures. Paik *et al.* [28] conducted research to determine the ultimate strength of plate structures with initial cracks subjected to axial loads, both compression and tension. Paik *et al.* [28] employed experimental and numerical methods to determine the ultimate strength of cracked steel plates. Numerical studies were conducted using nonlinear FEA. In his research, he varied the size and location of crack damage experimentally and numerically (Figure 5).

Paik *et al.* [28] showed that crack damage significantly reduces the ultimate strength of plates in experimental and numerical analyses using ANSYS. Paik *et al.* [28] also stated that the size of the crack is inversely proportional to the ultimate strength, meaning that larger cracks result in lower ultimate strength. Furthermore, Paik *et al.* [28] noted that cracks in panels subjected to axial compression can close and then buckle. It is also possible that lateral deflection occurs due to initial deformation or additional localized loading outside the plane of the plates. After buckling, lateral deformation is almost certain to occur. In the case of lateral deformation, cracks also reduce the ultimate strength of the panel as deformation outside the plane increases. The influence of crack damage on the ultimate compressive strength of the plate is similar to its effect on the ultimate tensile strength of the plate.

Paik [29] then continued his research with experimental and finite element methods (FEM) in two separate studies to determine the residual ultimate strength assessment of cracked plates, focusing on longitudinal cracks. The geometry of the plates used is shown in Figure 6(a), with the *x*-axis in the longitudinal direction and the *y*-axis in the transverse direction. Four variations of longitudinal cracks are used, as shown in Figure 6(b). The experimental results from the study by Paik [29] revealed that longitudinal center cracks, although relatively rare in real-world cases, exhibit a significant reduction, which is 7% of the ultimate compressive strength reduction when $2c/b = 0.5$. In addition, it has been observed that transverse cracks in steel plates have the potential to propagate when subjected to longitudinal axial tension, leading to a consequent reduction in ultimate strength. The most common location for crack occurrence is longitudinal edge cracks, particularly at the weld intersection between the plate structure and support elements.

In a subsequent study using FEA with the same configuration as the experimental research, Paik [30] stated that longitudinal center cracks do not cause a significant reduction in the ultimate strength of the plate, regardless

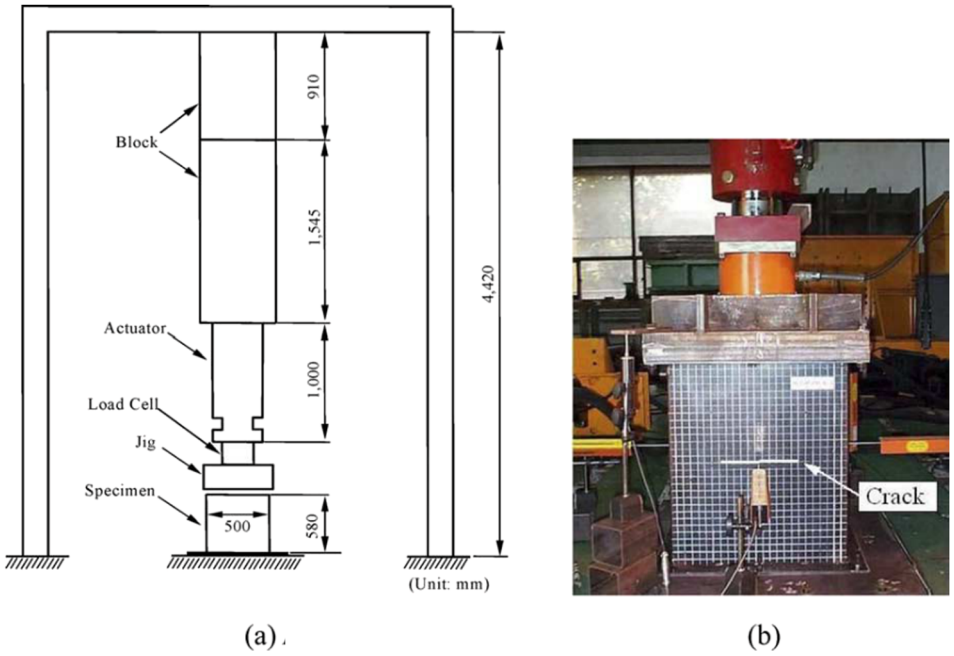

Figure 5: Experimental setup of Paik [28]. (a) A schematic view of the test set-up and (b) a photo of the test set-up.

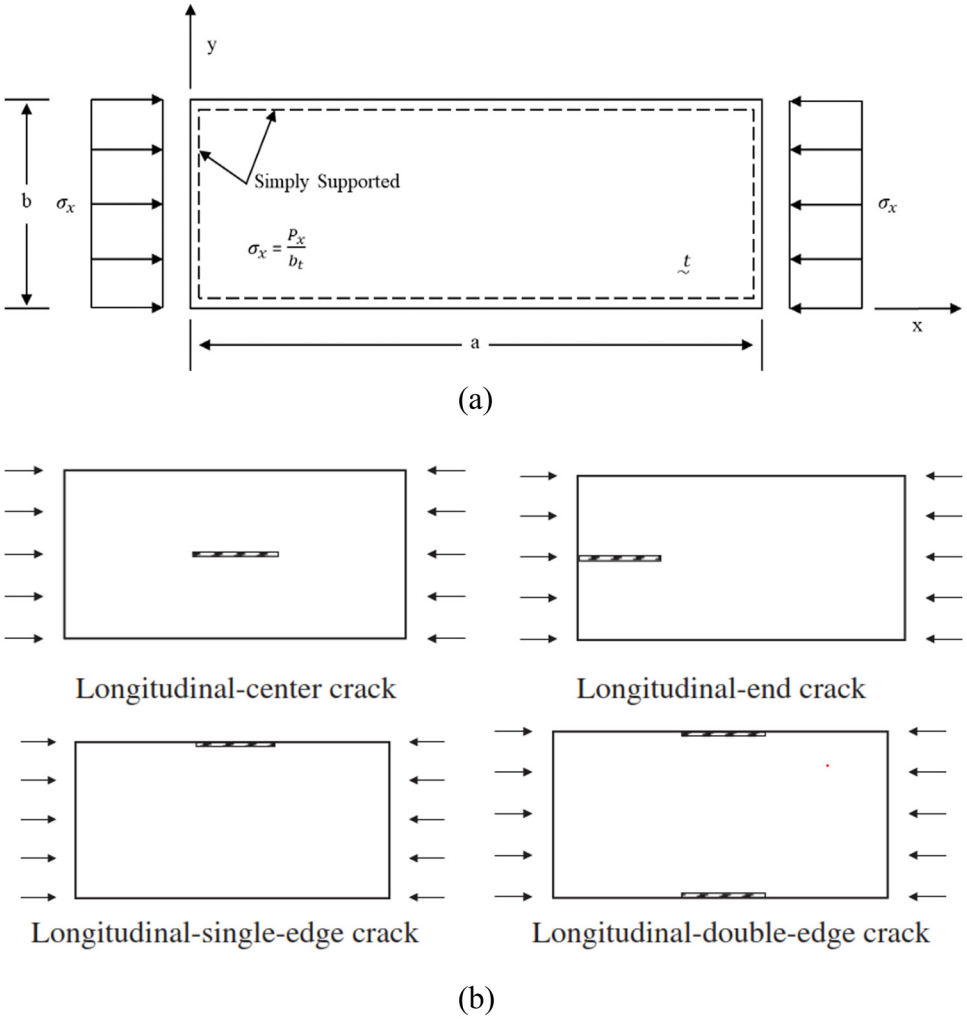

Figure 6: Configuration of (a) plate and (b) crack [29].

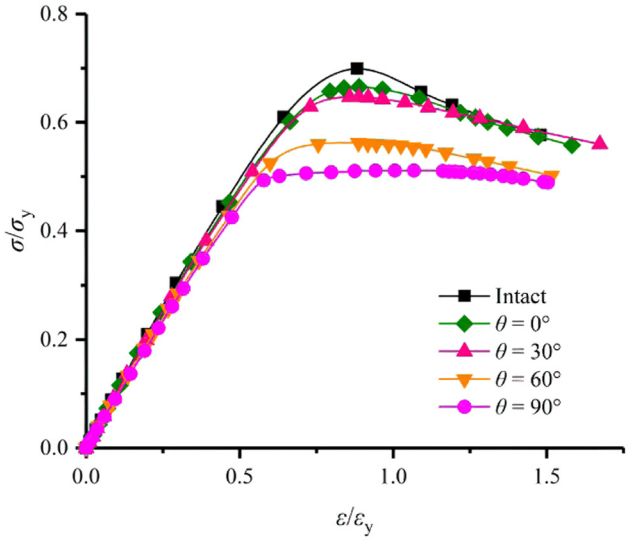

Figure 7: Ultimate strength graph on the effect of the crack angel [31].

of the crack size when $2c/b < 0.5$ under longitudinal compression. A similar trend was observed for longitudinal end cracks when $2c/b < 0.5$. However, Paik [30] mentioned that longitudinal end cracks result in a slightly more significant decrease in the ultimate strength of the plate.

Further research on the analysis of ultimate strength with imperfection cracks was conducted by Li *et al.* [31]. The analysis was performed using the FEM with ABAQUS software, and the results were verified by comparing them with the previous research conducted by Paik [30]. Li *et al.* [31] concluded that larger crack sizes lead to a decrease in the ultimate strength of the plate. Ultimate strength also inversely correlates with the crack angle, whereas when the crack approaches a transverse position, the ultimate strength decreases, as shown in Figure 7. In addition, considering factors such as longitudinal and transverse cracks and slenderness, it can be concluded that the reduction in ultimate strength due to transverse cracks is higher as the

plate slenderness increases compared to longitudinal cracks with the same slenderness rate.

Furthermore, Li *et al.* [32] continued their research by incorporating a new method for comparison. Li *et al.* [32] conducted analyses using the nonlinear FEM and artificial neural network (ANN). The research also considered the influence of crack orientation angles, lengths, longitudinal and transverse positions of multiple cracks, as well as the plate slenderness ratio on the plate strength characteristics. The geometry used by Li *et al.* [32] is shown in Figure 8, with values of a = 2,400 mm and b = 800 mm. The elastic modulus and Poisson's ratio were 205,800 MPa and 0.3, respectively.

The research results indicated that the data obtained from the FEA method using ABAQUS were consistent with and aligned with the results obtained from the ANN method. The formulas derived can also assess residual ultimate strength. From the data obtained, the ultimate strength decreases significantly as the crack angle between the side and longitudinal direction increases. The reduction in ultimate strength is most prominent when the crack is in the transverse position. Li *et al.* [32] also stated that an increase in crack length reduces the plate's strength. The increase in plate slenderness also reduces the ultimate strength. The position factor is also important, where if the longitudinal crack is centered in the middle of the plate, the decrease in ultimate strength will be drastic. In the case of a transverse crack, the closer it is to the long side of the plate, the more noticeable the reduction in ultimate strength.

2.3 Analysis of plate with corroded condition

In addition to cracks, corrosion is another imperfection variable considered in ultimate strength analysis research. Given that marine structures or ship structures are frequently in direct contact with seawater, the likelihood and risk of corrosion increase. One type of corrosion is pitting corrosion, which, by inducing stress concentration in a structure, can compromise a ship's strength. Studies on plates with pitting corrosion have been conducted, considering variations such as depth of penetration (DOP), pit depth, pit shape, pit size, pit distribution, and location. The corrosion patterns vary, including conical, hemispherical, and ellipsoidal shapes.

Zhang *et al.* [33] conducted a study on the ultimate strength of hull structural plates, considering pitting corrosion. Zhang *et al.* [33] modeled and analyzed pitting corroded plates using the FEM. In addition to pitting corrosion, Zhang *et al.* [33] considered residual stresses, taking into account that ship hulls are welded structural plates. In modeling the distribution of corroded pits, Zhang *et al.* [33] approximated uniformly distributed pits on the plate surface and assumed that the plate only rusted on one side. The loading applied in the study was combined loading, with a schematic shown in Figure 9.

Zhang *et al.* [33] indicated that the total corroded volume loss reduces ultimate strength. However, with the same total corroded volume, pit depth, and surface area variations did not significantly affect ultimate strength.

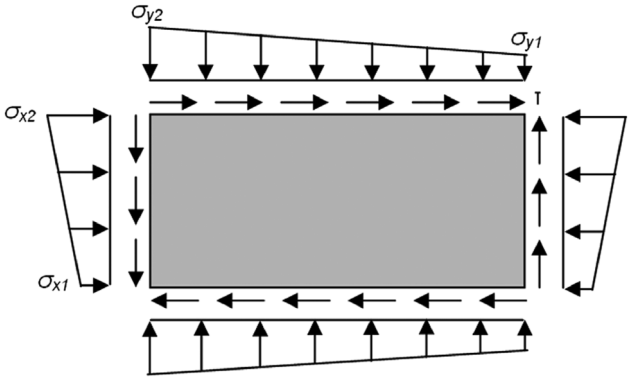

Figure 9: Schematic combined longitudinal and transverse load [33].

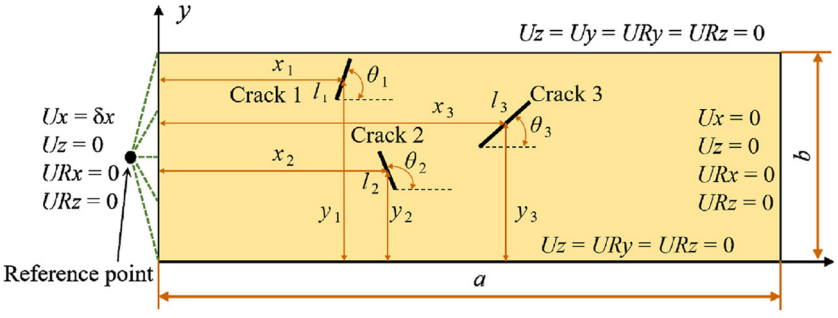

Figure 8: Plat and crack configuration [32].

The study also showed that the ratios between transverse and longitudinal stress and the ratios between shear and longitudinal stress influence the decrease in ultimate strength alongside the corroded volume. As shown in Figure 10, it is evident that the shear-to-longitudinal stress ratio parameter has a more significant impact on reducing ultimate strength.

One of the studies on the ultimate strength analysis of corroded plates was conducted by Silva *et al.* [34]. Silva *et al.* employed the FEM to investigate the influence of random corrosion thickness distribution on ultimate strength. A total of 3,575 models of corroded plate surfaces were generated using the Monte Carlo method and subsequently analyzed using the FEM with dedicated finite element coding. An equation was derived through regression analysis to predict the strength reduction in line with the analysis results, and it exhibited good accuracy.

Experimental research was conducted by Zhang *et al.* [35] to compare the experimental ultimate strength results with those obtained from FEA. The experiments involved

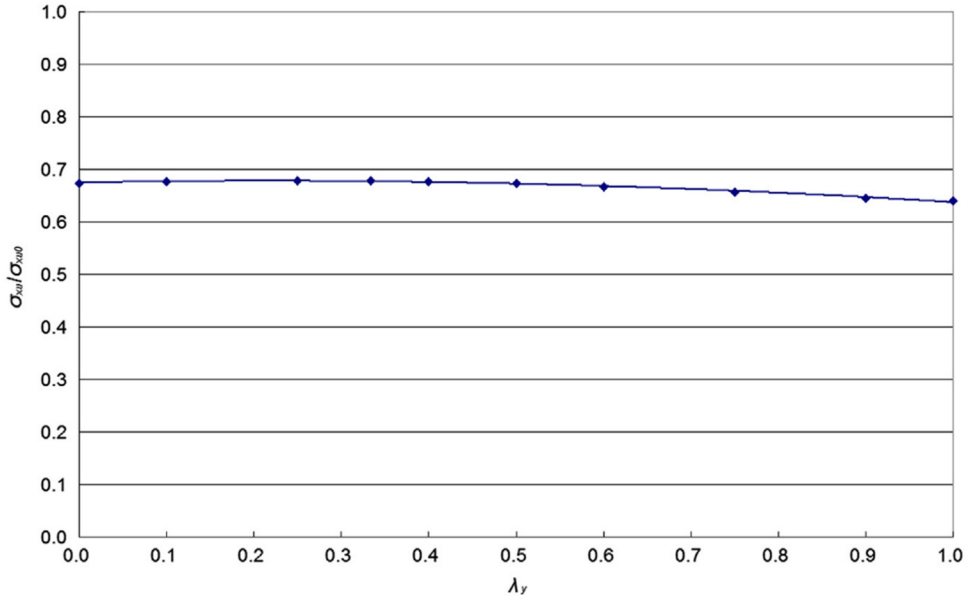

(a)

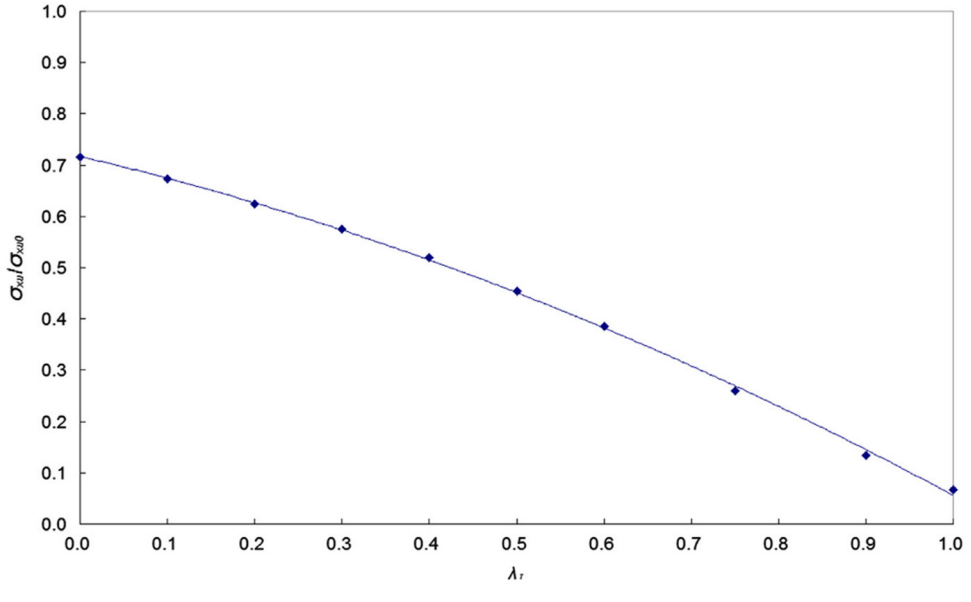

(b)

Figure 10: Relationship graph of ultimate strength and (a) longitudinal and transversal stress ration; (b) shear stress and longitudinal stress ratio [33].

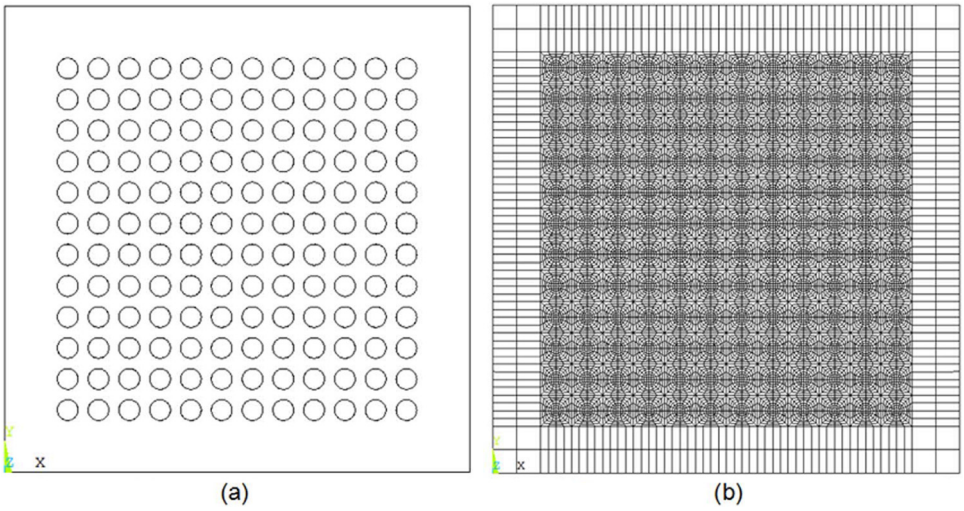

Figure 11: Corroded plate model [35]. (a) Pits distribution and (b) finite element model.

applying axial compressive loads to several plate samples using a specialized jig. The FEA models were assumed based on corrosion parameter measurements and calculations of corroded volume loss. The finite element models used are shown in Figure 11.

Due to the parameter matching between experiments and FEA, Zhang *et al.* [35] simplified the corroded pits as cylindrical pits with the same corroded volume loss, evenly distributed on the plate model in the FEA. To simplify calculations, the number of pits and their diameters were assumed to be the same. The results of this research showed that the difference between the ultimate strength values of plates with corrosion using experiments and FEA was less than 10%. Therefore, Zhang *et al.* [35] concluded that the research results are reliable. The results of the comparison between experiments and FEA are presented in Table 1.

Research on the ultimate strength of corroded plates has also been conducted under tensile loads. One such study was performed by [36], using non-linear implicit three-dimensional FEA with LS-DYNA coding. Ahmmad and Sumi [36] focused on determining the strength and deformability of steel plates with variations in pit sizes, degrees of pitting intensity, and general corrosion. A similar study was conducted by Nakai *et al.* [37]. The experiments showed that nominal tensile strength and elongation in corroded plates decreased. It was also found that pitting corrosion cases would reduce tensile strength more significantly than specimens corroded overall. Nakai *et al.* [37] further stated that tensile strength is more vulnerable to pitting corrosion than compressive and bending strengths.

In the case of general corrosion, comprehensive studies have also been carried out. General corrosion is a type of corrosion that frequently occurs in steel plate structures, as shown in Figure 12. Methods for simulating general corrosion vary from uniformly reducing plate thickness to using complex surface roughness. Generally, it is widely agreed that uniform corrosion patterns do not adequately reflect the local plastic hinge.

One study on general corrosion in plates was conducted by Khedmati *et al.* [38] using the FEM with a random thickness surface model. General corrosion was randomly distributed on one or both sides of the tested plate. The test results showed that variations such as slenderness and aspect ratio affect the characteristics of

Table 1: Comparison between experimental and FEA result [35]

Sample No	Experiment result		FEA result					Relative error	
	Corroded volume loss (mm)	Ultimate load (kN)	Number of pits	Pit diameter (mm)	Pit depth (mm)	Corroded volume	Ultimate load (kN)	Corroded volume loss (%)	Ultimate load (%)
1	155,152	220	144	20	3.4	153,812	228	−0.86	3.64
2	148,033	205	144	20	3.3	149,288	233	0.85	13.66
3	212,939	442	144	20	4.7	212,623	471	−0.15	6.56

Figure 12: Corrosion on ship plate [39].

corroded plates. In this study, Khedmati *et al.* [38] stated that corrosion occurring on one side of the plate slightly reduces ultimate compressive strength compared to corrosion occurring on both sides of the plate. The corrosion on the analyzed plate in the study by Khedmati *et al.* [38] is similar to the corroded plate in the experiment by Zhang *et al.* [39], depicted in Figure 12.

Another study by Rahbar-Ranji [40] focused on nonlinear FEA to determine the ultimate strength of corroded plates with irregular surfaces. The results were then compared with the ultimate strength of corroded plates with uniform surfaces and thickness. Corroded plates with irregular surfaces were assumed to have undulated surfaces, as shown in Figure 13. The plate thickness was varied, and the

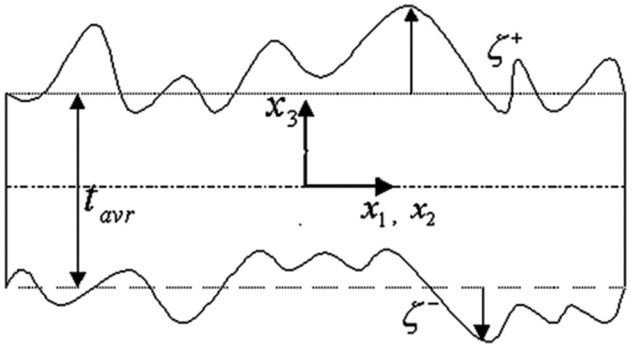

Figure 13: Undulated model of plate surface [40].

spacing between variation points was determined using the Monte Carlo method.

The results obtained align with the findings in the study by Khedmati *et al.* [38], where the reduction in ultimate strength due to corrosion is quite sensitive to the slenderness ratio and somewhat less sensitive to the aspect ratio. Ahbar also stated that the strength values for random corrosion are higher than or equal to those for uniform corrosion at low corrosion levels.

While most ultimate strength analyses are conducted using axial loading, such as compressive or tensile loads, the ultimate strength of ships can also be determined using combined loading, as demonstrated in a study by Cui *et al.* [18]. Cui *et al.* [18] employed a simplified analytical method proposed by Fujita *et al.* [41] by extending and modifying the method to apply to plates subjected to combined loading conditions. The equations used were then compared with existing references. Cui *et al.* [18] concluded that transverse compressive stress linearly reduces longitudinal ultimate strength. Cui *et al.* [18] stated that lateral pressure has a minimal effect on ultimate strength, which was compared with experimental results, showing good agreement.

In addition to the study by Cui *et al.* [18], Fujikubo *et al.* [42] estimated the ultimate strength of bottom plating subjected to transverse forces and lateral pressure. A deflection analysis was conducted by Fujikubo *et al.* [42] to assess the influence of lateral pressure on the plate. From the results obtained, Fujikubo *et al.* formulated an estimation formula for ultimate strength. The analysis was performed using a series of nonlinear FEM analyses. The analysis results showed a reduced normalized strength with increased transverse thrust and lateral pressure. Fujikubo *et al.* [42] compared between the FEM analysis and the equations derived in the study demonstrated good agreement, especially for thin plate thicknesses.

In its further development, the structure of ships with better strength is continuously researched, and one of the approaches involves the application of composite materials to achieve the desired properties and strength. One prevalent application of composites is the utilization of polymer composites for ships [43]. This practice has been increasingly adopted since the 1980s, primarily for military purposes aiming to reduce maintenance costs and attain superior structural strength. Composite materials, such as sandwich panel configurations, have been widely employed, notably exemplified by the Visby Corvette ships. These vessels incorporate carbon and glass fiber surfaces, resulting in weight reduction of over 30%. One notable study on the use of plate structures was conducted by Ma and Mahfuz [44]. They employed finite element simulation coupled with

fluid–structure interaction on ship sandwich plate structures. The core material of the sandwich structure utilized in their research was polyvinyl chloride foam. In addition, carbon/epoxy material layers were applied to withstand wave and blast loads. Stress analysis has shown that the core–skin interface near the girder is identified as the most susceptible area in sandwich plate structures. Interlaminar shear stress at this location exceeds the average core shear stress by approximately 27%.

In general, considering the plate structure as a crucial component in ships, a multitude of research studies have been conducted on plate structures encompassing various parameters and research methodologies. Further research is imperative for analyzing and advancing plate structures and their ultimate strength estimation in the future. All the studies discussed earlier can be found in Table 2.

3 Stiffened panel

Stiffened panels have been widely employed in ship construction due to their ability to enhance structural strength and safety without significantly increasing weight [45]. The addition of stiffened panels is crucial in reinforcing a ship's structure against sagging and hogging effects. In such conditions, the ship's structure experiences compression, especially in the longitudinal and transverse stiffener sections. Therefore, studies on stiffened panels can be categorized within structural engineering. Stiffened panels come in various geometric variations, primarily differentiated by the type of stiffener used. Tee-bars, flat-bars, and L-bars are examples of geometric variations for stiffened panels. Recently, extensive research has been conducted to evaluate the structural integrity of stiffened panels. Several studies have aimed to assess the strength of stiffened panels, with ultimate strength value being one of the key parameters for evaluation. When calculating the strength or ultimate strength value of stiffened panels, several critical geometric parameters, such as plate and column slenderness, are important references that can significantly influence the strength of stiffened panels.

3.1 Various methods for analyzing stiffened panel

Various methods have been employed to calculate the ultimate strength value of stiffened panels. Currently, research on stiffened panels subjected to axial compression has advanced, especially with the development of numerical solutions facilitated by technological advancements. Nevertheless, previous methods, particularly experimental methods, continue to be developed to validate the results of other analysis methods. Experimental research on stiffened panels has been conducted by Xu and Soares [46] using wide stiffened panels consisting of four stiffeners. The results of these experimental tests were compared with numerical method developments and methods specified in the CSR. Three different boundary conditions and three types of measurable initial imperfections, namely local, column, and torsional imperfections, were considered for all specimens in each testing method. In the study, the predicted ultimate strength values from CSR were the lowest, while the three results from numerical simulations or the FEM yielded higher values than the experimental results due to the influence of welding residual stress and fabrication.

Experimental research conducted by Xu and Soares [46] had previously been carried out by Xu and Soares [47] using the stiffened panel geometry of an oil tanker with a ½ + 1 + ½ bays model configuration. In Figure 14, 15 strain gauges were installed on the panel, with four of them positioned on the stiffener and the rest on the plate's surface.

In the experimental method conducted by Xu and Soares [47], a 300-ton hydraulic press was utilized to apply uniaxial compression forces, as shown in Figure 15. A simply supported condition was applied to the edges of the panel. With this setup, the maximum average stress during each loading cycle remained below the material's yield stress.

Hu *et al.* [48] conducted experiments using full-scale stiffened panels with three categories of variations: "as-built," "dented," and "damaged." Testing was performed by combining in-plane and lateral loads with symmetric boundary conditions. The results differed among the three variations applied to the stiffened panel, as shown in Table 3. The study's findings indicated that the "damaged" specimen dimensions exhibited different and inconsistent behavior compared to the "undamaged" specimen.

Over time, the development of experimental testing on stiffened panels has evolved by considering various other effects from actual conditions. Zhang *et al.* [35] studied the influence of pitting corrosion on stiffened panels subjected to compression loads. Variations in pit location and diameter affected strain distribution and led to changes in buckling positions. Pit location principally serves as the point of initial deformation when a stiffened panel is subjected to a load. The degree of pit corrosion (DOP) had the most significant influence in reducing the ultimate strength

Table 2: Studies related to ultimate strength analysis of ship plate

Test type	Material	Analysis method	Author	Title	Important remarks	Year
Transversal and lateral pressure	Steel	Nonlinear FEM	Fujikubo *et al.* [42]	Estimation of ultimate strength of ship bottom plating under combined transverse thrust and lateral pressure	Fujikubo *et al.* conducted an estimation of finite element strength and proposed an equation, then compared it with the FEM. The results showed alignment and acceptability	1999
Combined loading	Steel	Analytical method	Cui *et al.* [18]	Strength of ship plates under combined loading	The utilization of the analytical method proposed by Cui *et al.* is acceptable, considering the research findings and comparisons Transverse compressive stress linearly decreases longitudinal ultimate strength Lateral pressure has a minimal effect on ultimate strength	2001
Axial compression and tension	Steel	Experiment and FEM	Paik *et al.* [28]	Ultimate strength of cracked plate elements under axial compression or tension	Crack damage, crack size, and position significantly reduce both tensile and compressive ultimate strength The utilization of experimental methods in analyzing ultimate strength through the box compression test	2005
Axial compression	Steel	Experiment	Paik *et al.* [29]	Residual ultimate strength of steel plates with longitudinal cracks under axial compression–experiments	Experiments using the same method as before but with an emphasis on the type and variations of longitudinal crack locations	2008
Axial compression	Steel	FEM	Paik [30]	Residual ultimate strength of steel plates with longitudinal cracks under axial compression – nonlinear FEM investigations	Crack analysis using FEM with an emphasis on the types of cracks and variations in longitudinal crack locations	2009
Axial compression	Steel	Finite element method	Zhang and khan [21]	Buckling and ultimate capability of plates and stiffened panels in axial compression	FEA of ultimate strength in compressed plates. The results are used for formula development and compared with results obtained using Faulkner's equation for validation	2009
Quasi-static tensile load	Steel	FEM	Ahmmad and Summi [36]	Strength and deformability of corroded steel plates under quasi-static tensile load	The analysis is conducted using non-linear implicit three-dimensional FEA with LS-DYNA coding The results of the experiments show that the nominal tensile strength and elongation of corroded plates decrease. It is also noted that pitting corrosion cases result in a greater reduction in tensile strength compared to specimens corroded uniformly	2010
Uniaxial compression	Steel	Finite element analysis	Khedmati *et al.* [38]	A comparative computational investigation on the effects of randomly distributed general corrosion on the postbuckling behavior of uniaxial loaded plates	The analysis is carried out using FEM with a random thickness surface model, considering general corrosion. This is done on both one and both sides of the plate	2012

(Continued)

Table 2: *Continued*

Test type	Material	Analysis method	Author	Title	Important remarks	Year
					The results indicate that corrosion occurring on one side of the plate slightly reduces the ultimate compressive strength compared to corrosion occurring on both sides of the plate	
In-plane compression	Steel	Non-linear FEA	Rahbar-Ranji [40]	Ultimate strength of corroded steel plates with irregular surfaces under in-plane compression	Conducting ultimate strength analysis of plates with irregular surfaces using the Monte Carlo method to generate surface patterns	2012
Uniaxial compression	Steel	FEM	Silva *et al.* [34]	Ultimate strength assessment of rectangular steel plates subjected to a random localized corrosion degradation	Corroded plate modeling is conducted using Monte Carlo simulations to obtain a randomized corroded surface	2013
Combined loading	Steel	Nonlinear finite element analysis	Zhang *et al.* [33]	Ultimate strength of hull structural plate with pitting corrosion identification under combined loading	The analysis is performed considering the total corroded volume with pit surfaces simplified as cylinders	2016
Uniaxial compression	Steel	FEM and experiment	Zhang *et al.* [35]	Ultimate strength experiment of hull structural plate with pitting corrosion damage under uniaxial compression	Analysis is conducted using the FEM and experiments, with a comparison between experiments and simulations for pitting corrosion variables	2017
				Yan	Experiments are conducted using a specially designed jig Pits distribution is done uniformly by equalizing corroded volume loss	
Axial compression	Steel	FEM	Li *et al.* [31]	A study on residual ultimate strength of steel unstiffened plate with a crack	Ultimate strength analysis of ship plates using the FEM with variations in the angle and size of cracks	2020

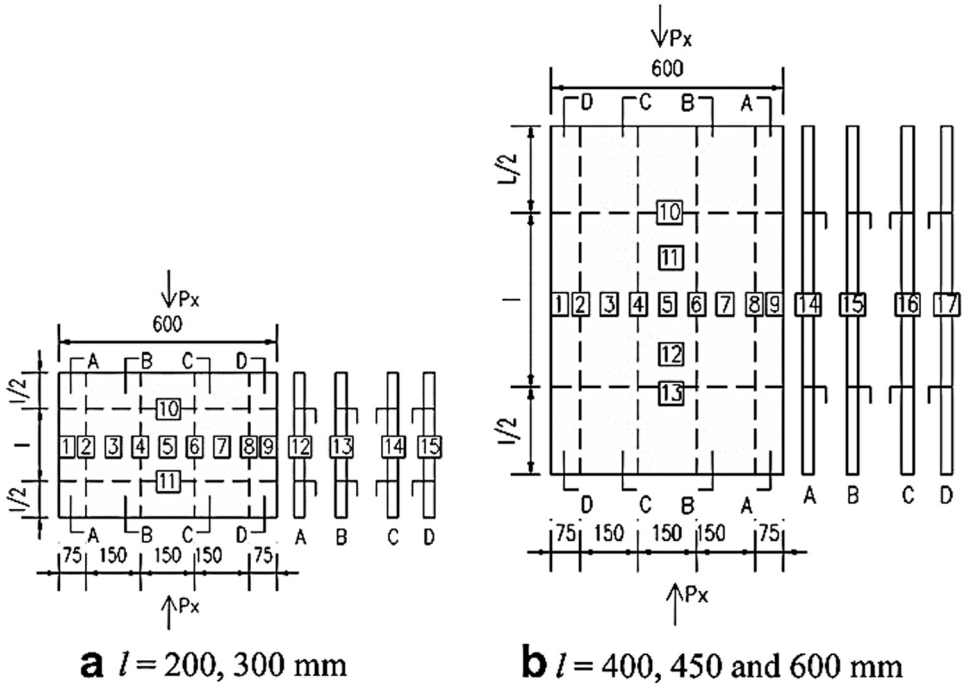

Figure 14: Geometry and strain gauge configuration with transverse frames space (*l*) [47]; (a) *l* = 200, 300 mm, (b), *l* = 400, 450, 600 mm.

value, while the effect of corrosion volume loss was minimal with the same DOP value.

Lin [49] formulated an equation that considered not only plate slenderness but also column slenderness, as shown in Eq. (9). Lin accounted for the influence of initial imperfections as local and torsional imperfections, and residual stress, with values of $b/200$, 0.0015, and $0.2\sigma_y$, respectively.

$$\frac{\sigma_U}{\sigma_y} = \frac{1}{\sqrt{0.960 + 0.765\lambda^2 + 0.176\beta^2 + 0.131\lambda^2\beta^2 + 1.064\lambda^4}}. \quad (9)$$

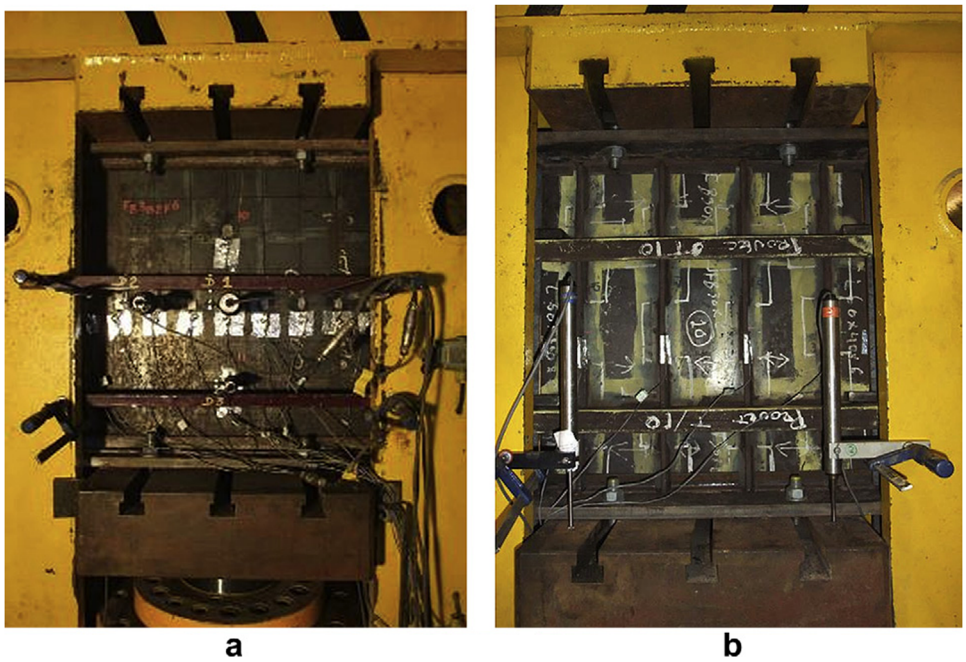

Figure 15: Experimental set up; (a) Initial set-up, (b) Hydrolic press installation [47].

Table 3: Summary of test result [48]

Specimen	Test variable			Test result	
	Dent/damage	Plate edge restaurant	Lateral load (kN)	Peak load (kN)	Buckling mode
SP 1.1	No	Yes	+10	1,572	Plate buckling followed by felxural buckling
SP 1.2	No	Yes	0	1,736	Plate buckling followed by felxural buckling
SP 1.3	No	Yes	+25	1,453	Plate buckling followed by felxural buckling
SP 1.4	No	Yes	−25	1,275	Stiffener tripping
SP 1.5	No	No	−25	1,134	Stiffener tripping
SP 1.6	No	Yes	−10	1,673	Stiffener tripping
SP 1.7	No	No	+25	1,361	Plate buckling
SP 2.1	20 mm	Yes	0	1,331	Plate buckling followed by felxural buckling
SP 2.2	35 mm	Yes	0	1,116	Plate buckling followed by felxural buckling
SP 3.1	In web	Yes	0	1,636	Local failure
SP 3.2	In flange	Yes	0	1,773	Plate buckling followed by felxural buckling
SP 3.3	In flange	Yes	0	1,683	Stiffener tripping

Paik and Thayamballi [50] provided a different formula with limitations on its use, as shown in Eq. (10). Twelve longitudinal stiffened panels were analyzed with different variations based on plate slenderness, accompanied by a single initial imperfection value of $b/200$. With the same limitations and considering column slenderness, Zhang and Khan [21] formulated a different formula to predict the ultimate strength value. Using a 1 + ½ + 1 bay −1 + ½ + 1 span model and providing local, torsional, and column imperfection modes with the same amplitude value, ultimate strength data through numerical simulations were collected. A range of geometric parameters, including plate slenderness ranging from 1 to 4.5 and column slenderness ranging from 0.25 to 0.9, were considered. The results were then used for proposing the formula presented in Eq. (11). In addition, various types of stiffeners (flat, L, and T) were considered. The results of predicting the ultimate strength for various types of stiffeners (flat, L, and Tee) based on numerical and analytical methods through the formula were compared, showing that 83% were within a margin of error of ±5 and 95.5% were within a margin of error of ±10%, as shown in Figure 16.

$$\frac{\sigma_U}{\sigma_y} = \frac{1}{\sqrt{0.995 + 0.936\lambda^2 + 0.170\beta^2 + 0.188\lambda^2\beta^2 + 0.067\lambda^4}} \leq \frac{1}{\lambda^2}, \tag{10}$$

$$\frac{\sigma_U}{\sigma_y} = \frac{1}{\beta^{0.28}\sqrt{1.0 + \lambda^{3.2}}}, \quad \text{for } \lambda \leq \sqrt{2}. \tag{11}$$

With the same goal of formulating a predictive formula for ultimate strength, Hanif *et al.* [51] introduced

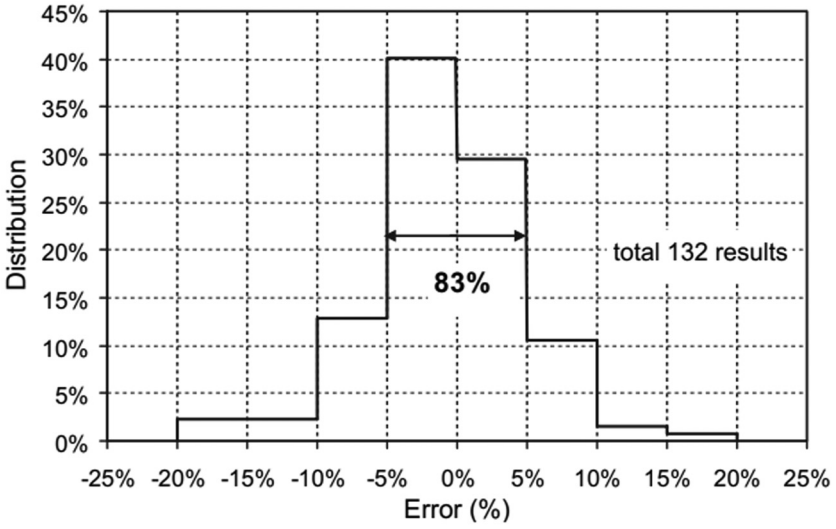

Figure 16: Comparison of error bands between the proposed formula and all FE results [21].

new variables. The research considered uncertainties in initial imperfections, including local, torsional, and column imperfection modes. The amplitude values for each imperfection mode varied, specifically 2.5, 25, 50, 75, and 100%, resulting in a large dataset from cross-combinations of amplitudes for each type of imperfection model. Through numerical analysis using Ansys APDL, the study also considered aspect ratio and web slenderness values, resulting in a predicted ultimate strength formula with a standard error of 2.08% compared to 750 data points analyzed using numerical methods, as shown in Figure 17. Furthermore, a comparison was also made with models of different geometries based on plate, web, and column slenderness values, resulting in Eq. (12) with a margin of error below 10%.

$$\frac{\sigma_U}{\sigma_y} = 0.682 - 0.322W_c - 0.154W_t - 1.580W_l - 0.025a/b + 0.370\beta_w + 0.074\lambda^3 - 0.01\beta^3\beta_w^3 + 0.069\beta_w^3\lambda^3, \text{ for } 1.9 \le \beta\beta_w \ge 3.3 \text{ and } 0.37 \le \lambda\beta_w \ge 0.88. \quad (12)$$

As mentioned earlier, FEM is one of the methods used to analyze and study a topic by utilizing computational capabilities in mechanics and mathematics. The use of numerical analysis can be performed without the need for complex manufacturing and preparation procedures, as required in experimental methods. The accuracy of the FEM method depends on various factors, and mesh density is one example of a factor that can affect the accuracy of the results obtained using the FEM method [52]. In their research, AbuBakar and Dow [52] used FEM to analyze and compare penetration damage in various grounding scenarios.

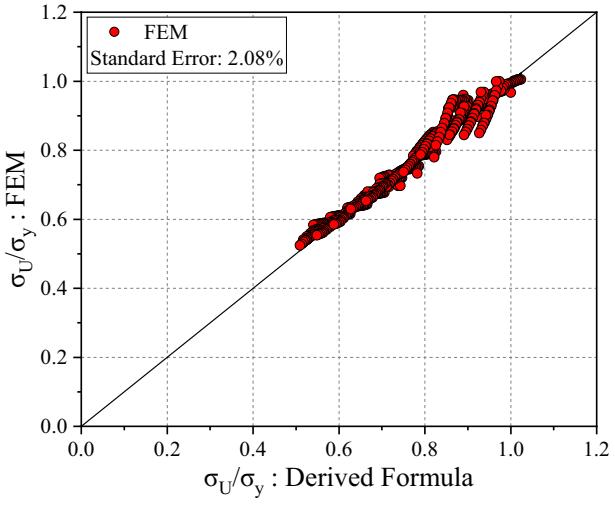

Figure 17: Comparison of derived formula to FEM [51].

In numerical analysis with compression loads, the FEM analysis is used to provide and modify various types of imperfections that can reduce the ultimate strength of the structure. Shi *et al.* [53] examined the influence of pitting corrosion by varying pit location, pit diameter, and pit depth on the ultimate strength of stiffened panel. The pit diameter ranged (d_c) from 20 to 60 mm, while the depth (t_c) ranged from 0 to $0.05t_0$ mm. The t_0 means the original thickness of stiffened panel. Parameters and pit locations are described in Table 4, and the pit shapes in the FEM illustration are shown in Figure 18.

As shown in Figure 18, the pit has a cylindrical shape and is located on only one side of the stiffened panel. The introduction of pit corrosion generally reduces the ultimate strength value by up to 20.7%. The largest reduction occurs in the T1 graph, as shown in Figure 19, which displays the load-end shortening curve of the stiffened panel with and without the influence of pit corrosion.

Through numerical calculation, Rigo *et al.* [54] conducted a sensitivity analysis on the ultimate strength of stiffened panels. In this study, L-type stiffened panels made of aluminum alloy were used under compressive loading. The loading was applied by imposing displacement in one direction while providing fixed constraints on the other side. The effect of reducing the yield stress in the heat-affected zone (HAZ) by 10% resulted in a decrease in ultimate strength ranging from 2 to 5%. Meanwhile, the effect of each millimeter of amplitude applied caused a reduction in ultimate strength of approximately 1.1%.

3.2 The influence of initial imperfection mode on stiffened panel

In both the studies by Shi *et al.* [53] and Rigo *et al.* [54], the analysis of stiffened panels considered the influence of

Table 4: Parameter and location of the pit [53]

Model	Pit diameter d_c (mm)	Pit thickness t_c (mm)	Number of pits	Pits distribution
L1	60	2.5	12	Left
L2	60	2.5	12	Center
D1	20	2.5	36	All
D2	60	2.5	36	All
T1	25	1	36	All
T2	25	3	36	All

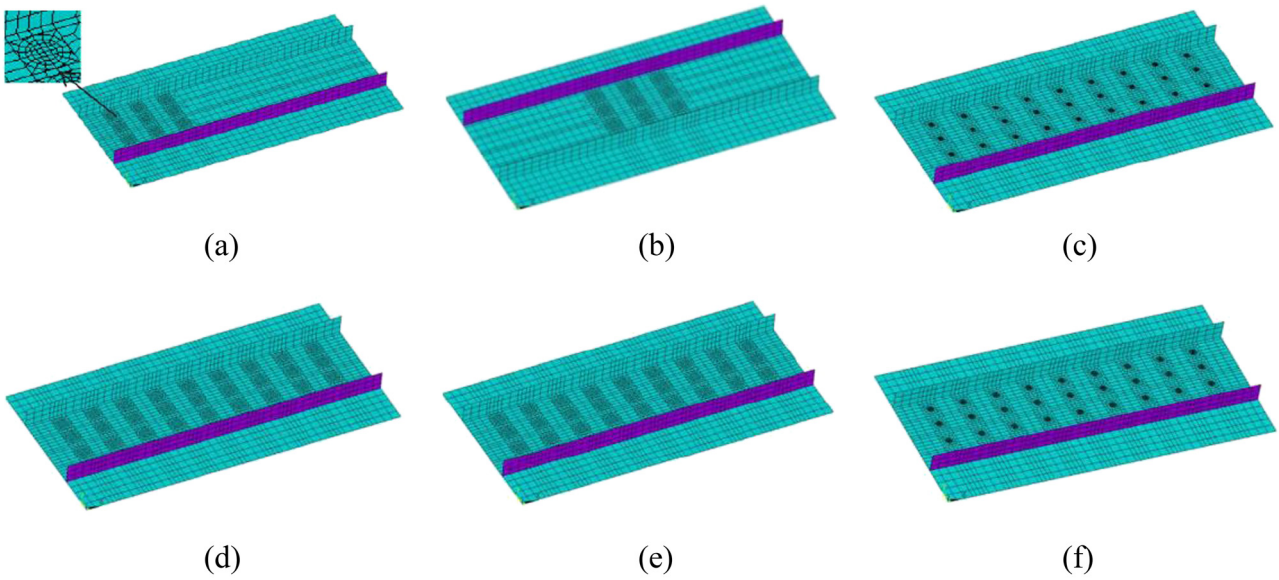

Figure 18: FEA model of stiffened panel [53]. (a) FEA Model-L1, (b) FEA Model-L2, (c) FEA Model-D1, (d) FEA Model-D2, (e) FEA Model-T1, and (f) FEA Model-T2.

initial imperfections. Using numerical methods, such analyses are feasible because of the flexibility offered by the method in modifying geometry. Anyfantis [55] introduced buckling imperfections into stiffened panels subjected to nonuniform thrust. Unlike Shi *et al.* [53], Anyfantis [55] used a ½ + ½ bay + ½ + ½ span model, as it was capable of modeling the specified buckling imperfections and applying simply supported conditions. Employing Ansys APDL, Anyfantis [55] introduced critical plate imperfections, local plate imperfections, column imperfections, and torsional web

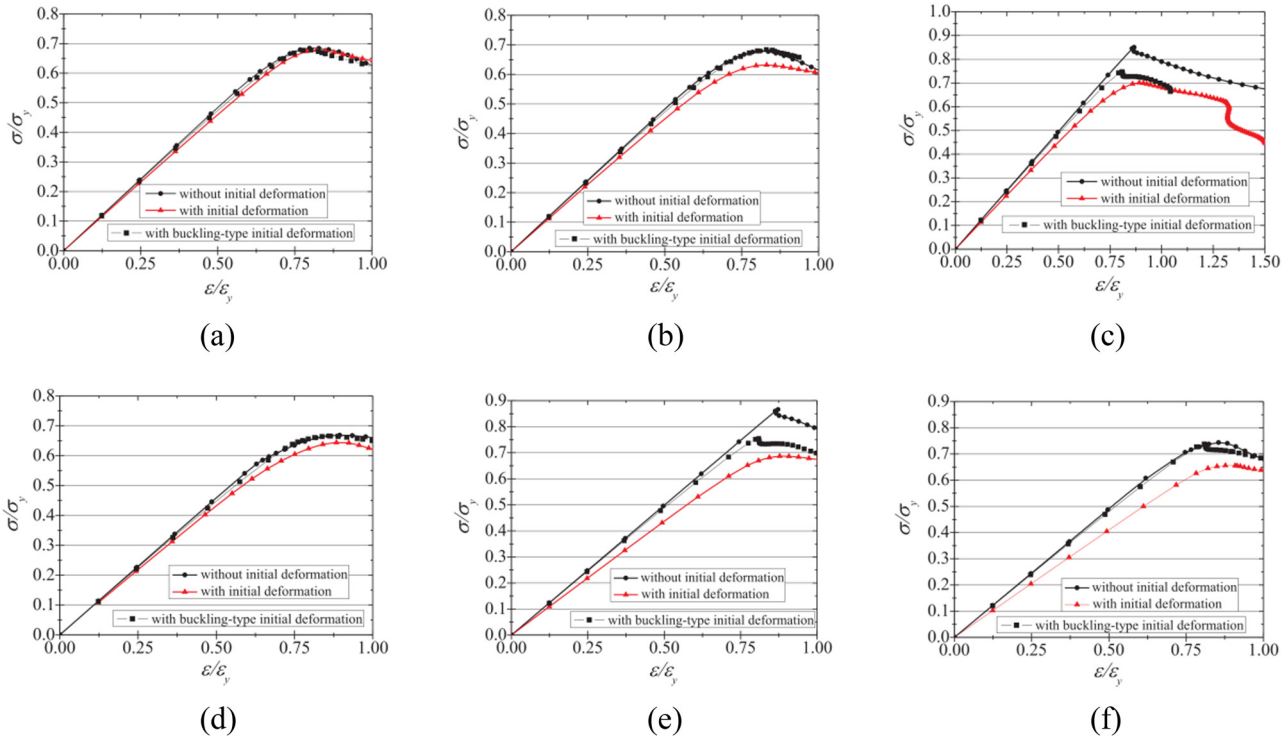

Figure 19: Stress–strain curves of the stiffened plates with pits [53]. (a) L1, (b) L2, (c) D1, (d) D2, (e) T1, and (f) T2.

imperfections. Global buckling imperfections also included tripping imperfection modes.

Similar to Anyfantis [55], Hanif *et al.* [51] conducted an analysis of stiffened panels with the influence of initial imperfections, including local, torsional, and column imperfections, as shown in Eqs. (13)–(15). The difference lies in the magnitude of the amplitudes applied. The overall illustration of imperfection modes is shown in Figure 20.

In Hanif's study [56], variations of amplitudes were applied at 2.5, 25, 100, and 300%. The percentage levels of initial imperfection severity refer to data provided by Fujikubo *et al.* [57], as shown in Figure 21. Values of 2.5, 100, and 300% indicate that the severity level falls within the slight, average, and severe ranges. The amplitude of the initial imperfection is determined by $\beta^2 t$ or the square of plate slenderness multiplied by plate thickness. The numerical results compared to analytical calculations outlined by IACS-CSR [58] found that the IACS ultimate strength predictions fell within the ultimate strength range for severity levels of 25–100%.

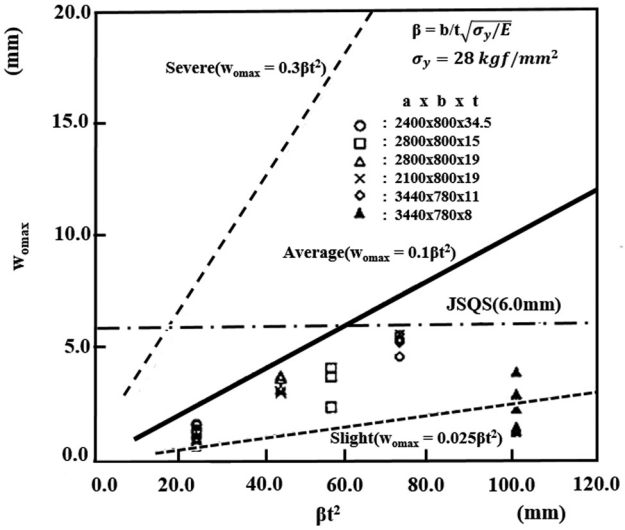

Figure 21: Analysis of scatter data of initial geometric imperfections. Reproduced from the study by Fujikubo *et al.* [57].

$$W_1 = C_0 \sin\frac{m\pi x_i}{a}\sin\frac{\pi y_i}{b}, \tag{13}$$

$$W_t = B_0 \frac{z_i}{hs}\sin\frac{\pi x_i}{a}, \tag{14}$$

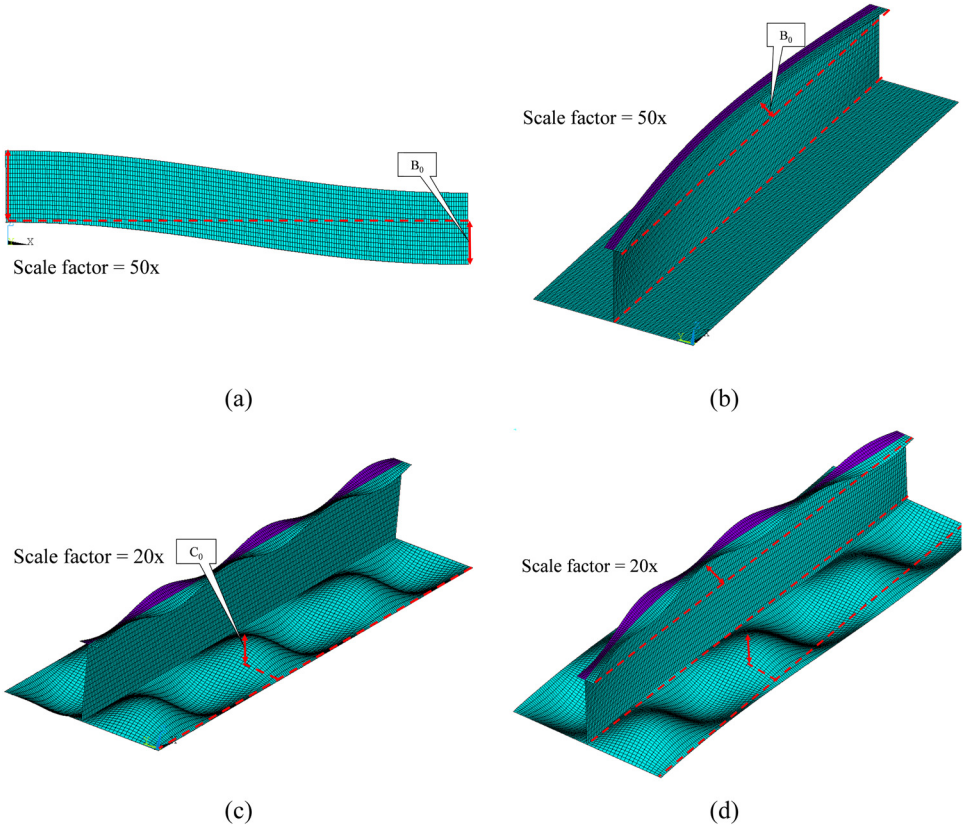

Figure 20: Illustration of the initial geometric imperfection modes applied to the stiffened panels: (a) column imperfection mode, (b) torsional imperfection mode, (c) local imperfection mode, and (d) combination of the three imperfection modes [51].

$$W_c = B_0 \sin\frac{\pi x_i}{a}. \tag{15}$$

Li *et al.* [59] introduced different types of imperfection modes applied to stiffened panels, including hungry-horse mode, Admiralty Research Establishment mode, and critical buckling mode. The study focused on assigning random amplitudes to each imperfection mode to understand the distribution of ultimate strength and buckling behavior exhibited by the stiffened panel. Equations for each imperfection mode are presented in Eqs. (16)–(18).

$$w_{\text{opl}} = w_{\text{opl}}^{\max}\sum_{i=1}^{11} A_{0i}\sin\left(\frac{i\pi x}{a}\right)\sin\left(\frac{\pi y}{b}\right), \tag{16}$$

$$w_{\text{opl}} = w_{\text{opl}}^{\max}\left\{A_1\sin\left(\frac{\pi x}{a}\right) + A_j\sin\left(\frac{j\pi x}{a}\right) + A_{j+1}\sin\left[\frac{(j+1)\pi x}{a}\right]\right\}\sin\left(\frac{\pi y}{b}\right), \tag{17}$$

$$w_{\text{opl}} = w_{\text{opl}}^{\max}\sin\left(\frac{m\pi x}{a}\right)\sin\left(\frac{\pi y}{b}\right), \tag{18}$$

$$j = \frac{a}{b} + 1, \tag{19}$$

$$\frac{A_1}{A_j} = 4.0, \tag{20}$$

$$A_{j+1} = 0.01, \tag{21}$$

$$\frac{a}{b} \le \sqrt{m(m+1)}. \tag{22}$$

The magnitude assigned in the study refers to research conducted by Smith *et al.* [60], where the amplitude value is a function of $\beta^2 t$. Referring to the same graph provided by Fujikubo *et al.* [57], the severity levels assigned are 25% or slight condition, 100% or average condition, and 300% or severe condition. The stochastic geometric imperfections applied are obtained from the study conducted by Georgiadis *et al.* [61] for local plating, as shown in Figure 22. The results of the stochastic geometric imperfection model demonstrate its ability to determine the imperfection model based on the maximum distortion magnitude and combine the effects between them.

Gandhi *et al.* [62] studied the influence of initial deflection on various types of stiffened panels based on their stiffener types (Tee and angle bar). In this study, only local and column imperfection modes were applied with a single-level severity amplitude of 100% referred to the first buckling mode between two stiffeners. Simply supported boundary conditions were applied to the model, where not all edges were fixed, but some degree of freedom was coupled to apply continuous conditions similar to the actual condition. The coupling provided freedom for the edge to deform in specific rotational directions. Using a 1 bay – 1 frame model, the study's results were accurate, validated by comparing them with numerical results from the ALPS - ULSAP and MSC MARC methods and also demonstrated that variations in stiffener size had a significant impact on normalized strength values. The choice of stiffener type, either Tee or angle Bar, did not show significant differences when observing the load-end shortening curve analysis.

Rizzo and Caire [63] introduced variations in initial imperfections in their stiffened panel analysis under combined compression and shear by employing a 1 bay – 3 span model with 3D modeling of the transverse stiffener. Before collecting data for analysis, a mesh convergence study on the stiffened panel was conducted and subjected to pure compression to obtain accurate and efficient results, as shown in Table 5. The combination of longitudinal compression and edge shear loading increased the ultimate strength value due to the influence of plastic hardening. The initial imperfections were introduced in the form of the first buckling mode on the damaged area, which was located in the middle of the plate. Further imperfections were introduced by applying a collision case caused by rigid

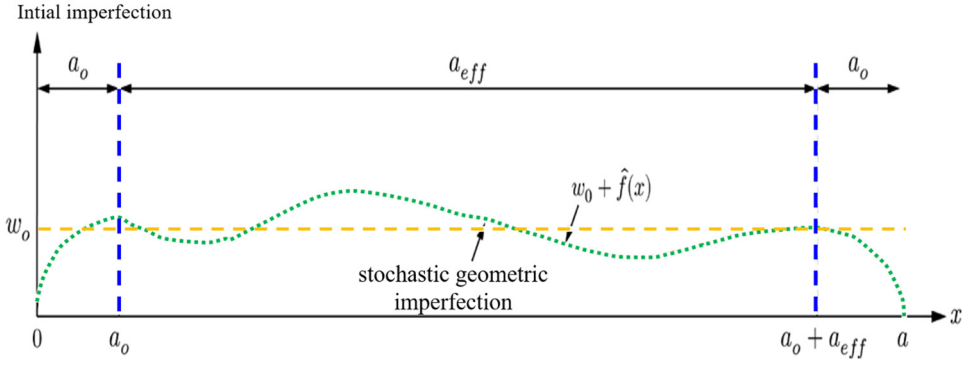

Figure 22: Schematics of stochastic geometric imperfection based on the information obtained from the study by Georgiadis *et al.* [61].

Table 5: Mesh sensitivity study under pure compression – load proportionality factor (LPF) [63]

Mesh	Plate (mm)	Stiffeners/frames (mm)	LPF
1	100 × 100	100 × 100	4.573
2	75 × 75	100 × 100	4.638
3	50 × 50	100 × 100	4.625
4	25 × 25	100 × 100	4.618
5	50 × 50	50 × 50	4.621
6	50 × 50	75 × 75	4.623

sphere indentation varied from 50, 100, 200, to 300 mm, as illustrated in Figure 23. Subsequently, a combination of loading was applied, with shear loading first, followed by longitudinal compression loading. As expected, the magnitude of the initial imperfection decreased the ultimate strength value, and in this case, the decrease in ultimate strength was more sensitive to compression than to shear load.

3.3 The influence of corrosion on stiffened panel

In addition to initial deflection and variations in buckling imperfection modes, initial imperfections in stiffened panels can occur due to corrosion. This is a potential issue considering the long-term activity of ships, which can lead to corrosion caused by air, seawater, and sea creatures. Feng *et al.* [64] analyzed the influence of pit degree (DOP), depth, location, and distribution of pit corrosion on the ultimate strength value when subjected to uniaxial compression. Three types of stiffened panels adopted from the research of Zhang and Khan [21] were used with a configuration of 11 bays and ½ + 1 + ½ span, as shown in Table 6. The transverse stiffener modeling in Feng *et al.*'s [64] study was given only a boundary condition in the form of fix constraints. In addition to corrosion effects, initial imperfections in the form of initial deflection in the form of local and global imperfection modes were also considered in the analysis. The pit diameter was 60 mm when evenly distributed, but for randomly distributed pits, the diameter ranged from 50 to 70 mm. As for the pit depth, the variations ranged from $0.33t_0$, $0.67t_0$, to $1.0t_0$, where t_0 represents the intact thickness value, while DOP was varied in three magnitudes: 5.98, 11.96, and 23.72%. The addition of DOP was associated with a significant reduction in ultimate strength, and this effect increased as the pit depth increased, as shown in Figure 24 upper graph. In this figure, it can be seen that with a low DOP of less than 7%, the effect of pit depth was minimal. Similar to the DOP effect, increasing the pit depth would reduce the ultimate strength value. However, based on the trend shown, a larger DOP would not significantly

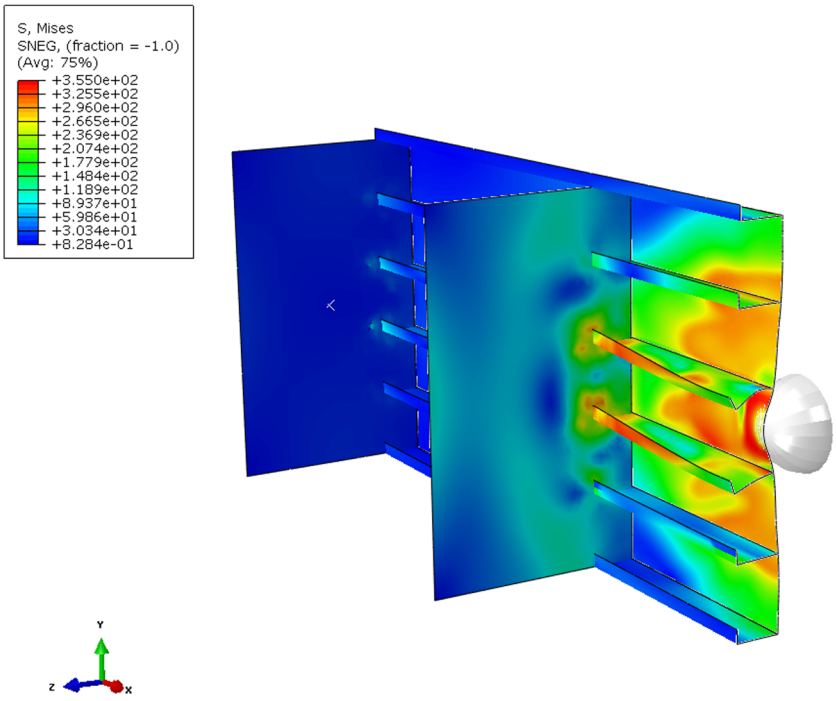

Figure 23: Stress distribution at maximum indentation – 200 mm displacement [63].

Table 6: Geometric dimensions of the three stiffened panel extracted from [21]

ID	Panel			Stiffener web		Stiffener flange		Stiffener type
	a (mm)	b (mm)	t (mm)	h_w (mm)	t_w (mm)	h_f (mm)	t_f (mm)	
1	3,500	810	15	300	11	90	16	L
2	4,500	815	18	463	11	172	17	T
3	5,500	910	19	400	12	100	18	L

affect the reduction in ultimate strength in models with different pit depths, as shown in Figure 24 lower graph.

The influence of random corrosion was analyzed on stiffened panels by Feng *et al.* [65] using the nonlinear FEM (NLFEM). Stiffened panels on the deck portion were used in this analysis without modeling the transverse stiffener. The randomness values of corrosion were obtained from 80 measurement data referring to 15 ships with different ages, with the statistical approach adopted from data obtained in Wang *et al.*'s [66] research. The ultimate strength values of randomly corroded panels followed a log-normal distribution. A Monte-Carlo approach was used to analyze the statistical characteristics of the ultimate strength of stiffened panels affected by corrosion. Corrosion data were obtained through the Monte-Carlo approach based on the log-normal model.

3.4 The influence of residual stress on stiffened panel

Another type of initial imperfection that can affect the load-bearing capacity of stiffened panels is residual stress, generally caused by heat imparted along the welded portion of stiffened panels. Li *et al.* [67] conducted research on the influence of residual stress on the ultimate strength of stiffened panels. Figure 25 shows the idealized welding-induced residual stress [67]. The distribution and magnitude of residual stress have been previously formulated by Smith and Anderson [68] through a simplified welding-induced residual stress distribution. With this configuration, residual stress was modeled as tension and compression blocks, as shown in Figure 25(a). Using a similar model, the distribution of residual stress was formulated by Yao

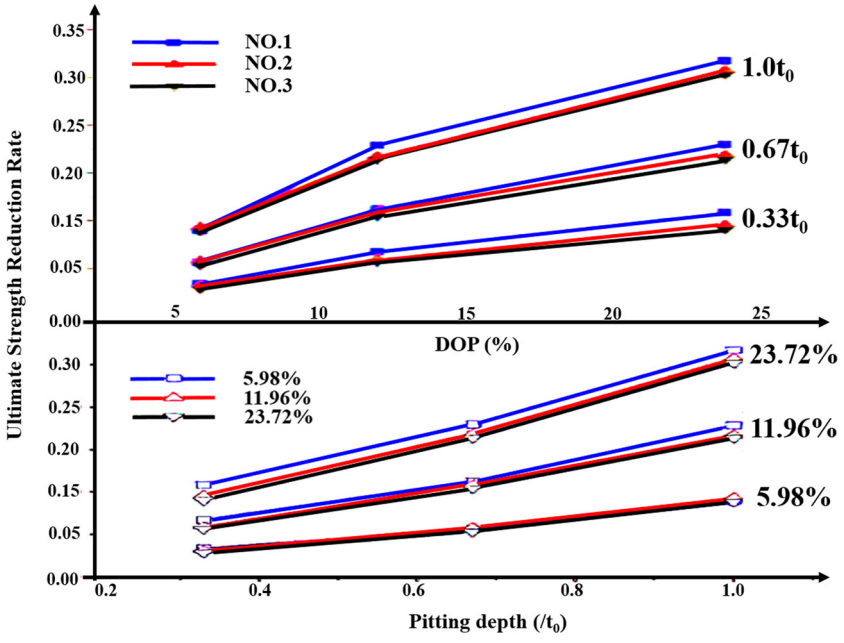

Figure 24: Strength reduction caused by DOP and pit depth based on the information obtained from Feng *et al.* [64].

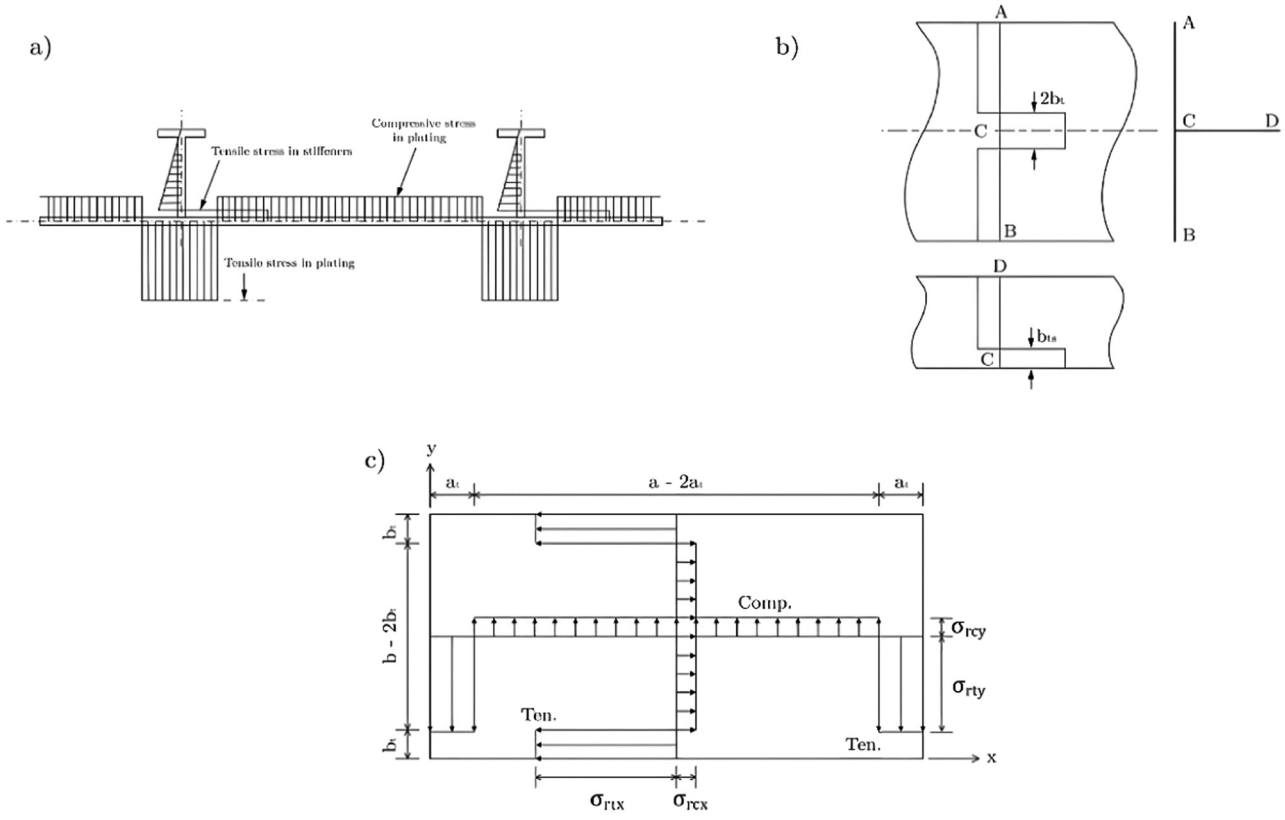

Figure 25: Welding-induced residual stress in stiffened panels [67]; (a) Simplified model, (b) Model for fillet welding, and (c) Bi-axial distribution for plating.

and Fujikubo [69] in Figure 25(b), but a uniform distribution was assumed for compression stress upward along the stiffener web. Paik and Thayamballi [70] formulated a different distribution of residual stress in Figure 25(c), with a bi-axial pattern considering residual stress in the longitudinal and transverse directions.

To account for the effects of residual stress, an edge function was formulated by Gordo and Soares [71] to modify the material behavior of stiffened panels with residual stress, resulting in the stiffness reduction by $1.0 - \varepsilon_{rcx}/\varepsilon_{Yeq}$. The initial edge function was modified to simulate material behavior as described sequentially in Eqs. (23a), (23b) and (24), which is also used in the CSR-H method.

$$\phi = \varepsilon/\varepsilon_y, \quad \text{if } \varepsilon/\varepsilon_y \le 1.0, \tag{23a}$$

$$\phi = 1 \text{ if }, \quad \varepsilon/\varepsilon_y > 1.0, \tag{23b}$$

$$\phi = \varepsilon/\varepsilon_y \text{ if }, \quad \varepsilon/\varepsilon_y \le 1.0 - \varepsilon_{rcx}/\varepsilon_y. \tag{24}$$

In their study, stiffened panels were categorized into three types: stiffened panels without residual stress, stiffened panels with residual stress in the local plate, and stiffened panels with residual stress in both the plate and web. The initial residual stress in this case was controlled using Eq. (21) developed by Yi *et al.* [72], where the width of the longitudinal tensile residual stress block is a function of plate slenderness (β) and weld leg length (L_w). However, in their study, the tensile residual stress was assumed to be equal to the yield stress of the material. The distribution applied followed that formulated by Paik and Thayamballi [70] but neglected the transverse direction. The results of the geometry illustrations affected by residual stress are shown in Figure 26.

The analysis results show that a significant reduction in ultimate strength occurs in almost all cases, and the effect of residual stress can lead to a reduction of up to 11.2% compared to stiffened panels without the influence of residual stress. Furthermore, the analysis results also indicate that collapse in stiffened panels generally occurs at higher strains. This is due to the effect of residual stress and becomes more sensitive in stiffened panels with low plate and column slenderness values. In addition, the application of residual stress does not alter the postcollapse behavior of stiffened panels. When applied only to the local plate, residual stress reduces the average ultimate strength by around 6%, but in combination with the plate and web, it ranges around 8.5%.

$$b_1 = c_1 \times L_w + d_1, \tag{25}$$

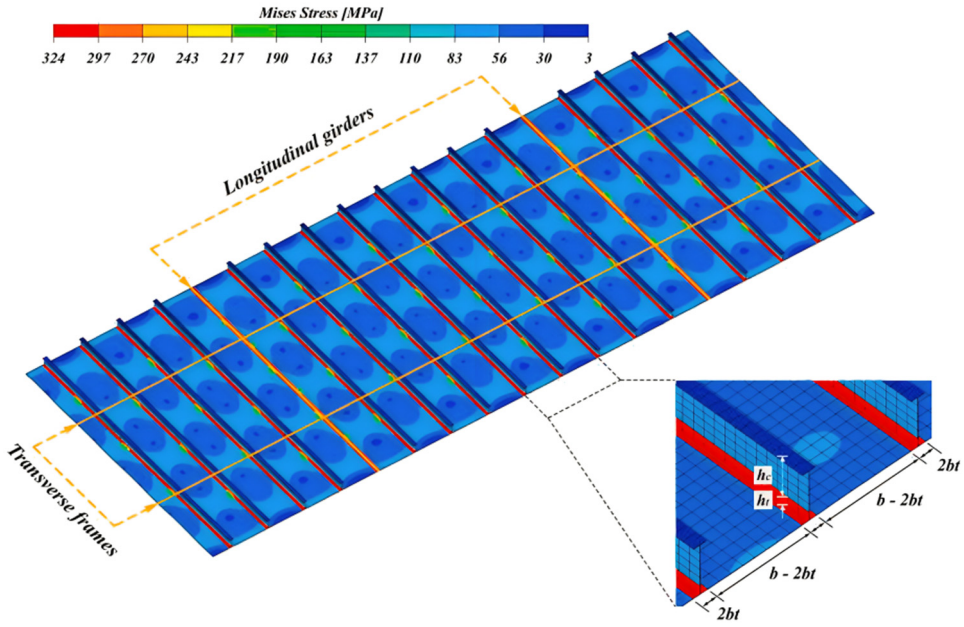

Figure 26: Stiffened panel after relaxation of the initial residual stress [67].

where

$$c_1 = -0.6212\beta^2 + 5.9145\beta - 3.3894, \quad (26)$$

$$d_1 = 1.9505\beta^2 - 16.234\beta + 18.711. \quad (27)$$

In parametric studies conducted by Grondin *et al.* [73], beside the variation in residual stress in terms of its magnitude, initial deflection and the direction of applying uniform bending and stiffened panel geometry were also introduced. Using ABAQUS, the flange and stem of the stiffener were divided into 96 elements, while the plate was divided into 384 elements to achieve the desired results. Modeling of residual stress was realized in simulations by imposing initial strains in the form of temperature distribution and applying only longitudinal residual stress. The

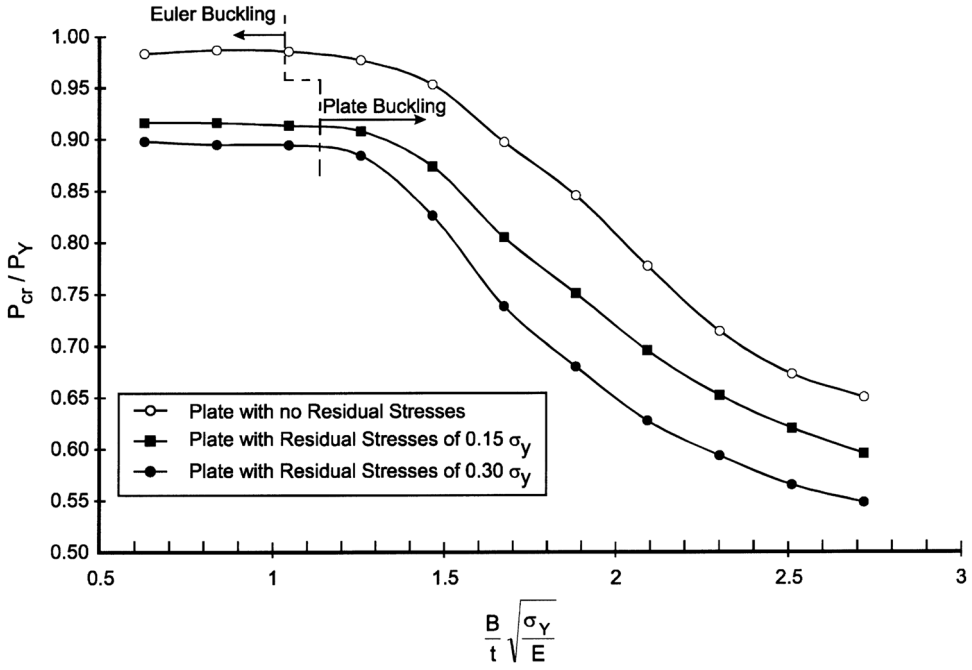

Figure 27: Effect of residual stresses [73].

imposition of initial strains in that direction was done by setting the thermal expansion to zero in the orthotropic temperature material property. The magnitude of residual stress at the junction between the plate and stiffener was given as the yield strength of the material in tension. To understand the effect, variations in magnitude were performed with values of 0, 15, and 30% of the yield strength. The effect of residual stress on the strength of the stiffened panel can be seen in Figure 27, which shows the normalized strength against plate slenderness ratio. In stiffened panel models with a plate slenderness greater than 1.7, a significant decrease in strength due to the effect of residual stress occurs.

On the other hand, Khan and Zhang [74] introduced the effect of residual stress on stiffened panels using the formula formulated by Faulkner [26], as shown in Eq. (28). For practical design and simulation purposes, similar to previous studies, the welding-induced stress distribution at the plate–stiffener junction was idealized by forming tensile and compressive stress blocks. In Faulkner's equation [26], the magnitude of the residual stress depends on the value of η, which in ship applications varies between 4, 5, and 6. In the shakedown value, the allowable value is 3 and 4.5.

Unlike the research described earlier, in the study by Khan and Zhang [74], residual stress values were set to be 0 and 0.25 of the yield strength. The value of η was set at 2.45, 4.99, and 6.4. By introducing another variation in plate thickness, as shown in Figure 28, the load-end shortening curve without residual stress exhibits a sharp decline after collapse, while the stiffened panel with residual stress tends to have a gentler decline after experiencing collapse at high strains. With increasing magnitude of residual stress, it can be observed in the graph that the "no load shedding zone" also increases. This occurs in each variation of plate thickness, whether it is 12.8, 17.8, or 21.3 mm.

$$\frac{\sigma_r}{\sigma_0} = \frac{2\eta}{\left(\frac{b}{t}\right) - 2\eta}. \tag{28}$$

3.5 The influence of crack on stiffened panel

The influence of other types of initial imperfections in the stiffened panel can also take the form of cracks. Typically, cracks are found along weld lines and intersections on stiffened panels. Analysis of stiffened panels with cracks has been conducted in both experimental and numerical analyses. Bayatfar *et al.* [75] studied the influence on stiffened panels subjected to longitudinal compression. A one bay–one span model was used in the analysis with a flat bar-type model of a stiffened panel. There were two variations of cases given for the stiffened panel. In the first case, the crack was located in the middle of the plate transversely and had a length of 10–50% of the plate width, while in the second case, there were two cracks on the stiffened panel. The first crack was in the middle of the plate with a length of 20% of the plate width, while the second crack was vertically positioned in the middle of the longitudinal web-plate junction. The length of the second crack ranged from 10 to 50% of the plate width. The graphs of the results from the first and second cases are shown in Figure 29. In

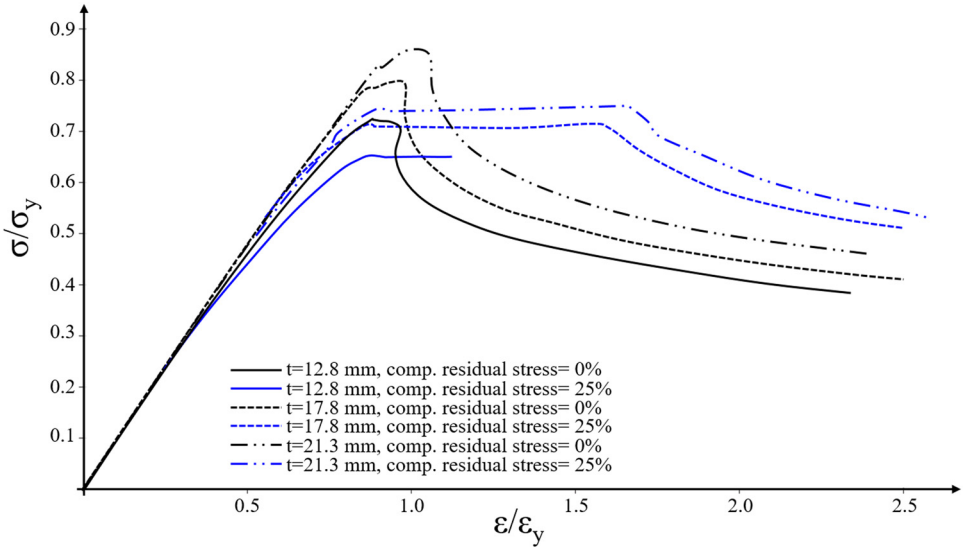

Figure 28: Load shortening curves of stiffened panel considering different values of compressive residual stress for 12.8, 17.8, and 21.3 mm plate thickness based on the information obtained from the study by Khan and Zhang [74].

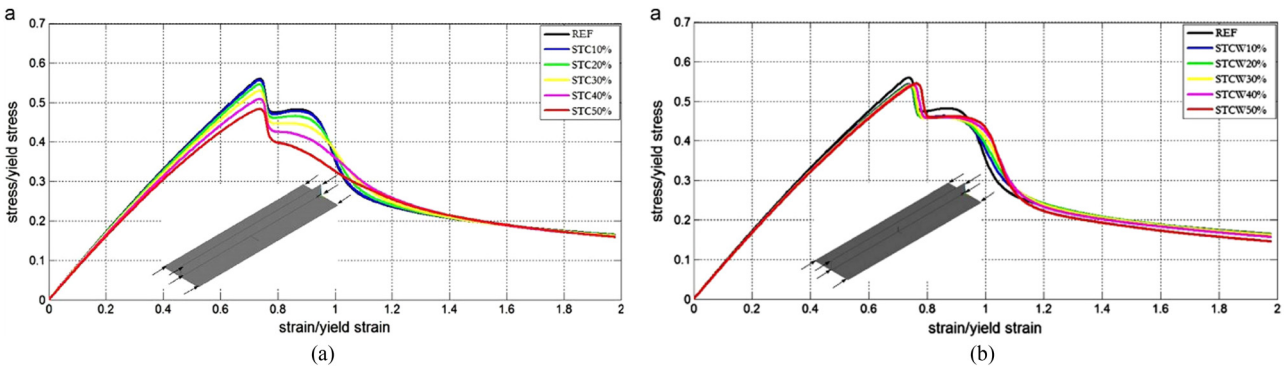

Figure 29: Nondimensional average stress–average strain curves: (a) case 1 and (b) case 2 [75].

Figure 29(a), it can be seen that the effect of crack length significantly reduces ultimate strength. In addition, local plastic deformation is concentrated in the middle area of the plate as the crack length increases. In the second case, the increase in the crack length in the web area does not significantly reduce the ultimate strength.

Using different loading test, Dexter and Pilarski [76] analyzed the effect of crack propagation on welded stiffened panels under four-point bending. Through experimental testing, two 490-kN actuators under load control were used to provide a constant load range as the crack propagated. Ten different types of stiffened panels were tested in the study, with variations in stiffener type, stress range, notch length, and stiffened panel crack detail. The results showed a reduction in the crack propagation rate due to the effect of compressive residual stress between the stiffeners.

In another study, Cui *et al.* [77] used cracks as the main parameter alongside providing other parameters such as initial deflection. Using NLFEM, four types of crack models were modeled, as shown in Figure 30. These models were distinguished based on the location of the crack. Initial A, B, P, and S have their meanings from the presented diagram, where P means the crack is located only in the plate, while S means the crack location is in both the plate and the stiffener. S refers to a symmetric crack location, while A refers to an asymmetric crack location relative to the stiffener. The variations in the crack length ratio to plate width were 0.1–0.4, while the crack length ratio in the stiffener to web height was 0.2.

Figure 31(a) plots ultimate strength values, which show a linear and significant decrease with the increasing crack length. It can be seen that adding a crack in the stiffener significantly reduces the ultimate strength, while adding

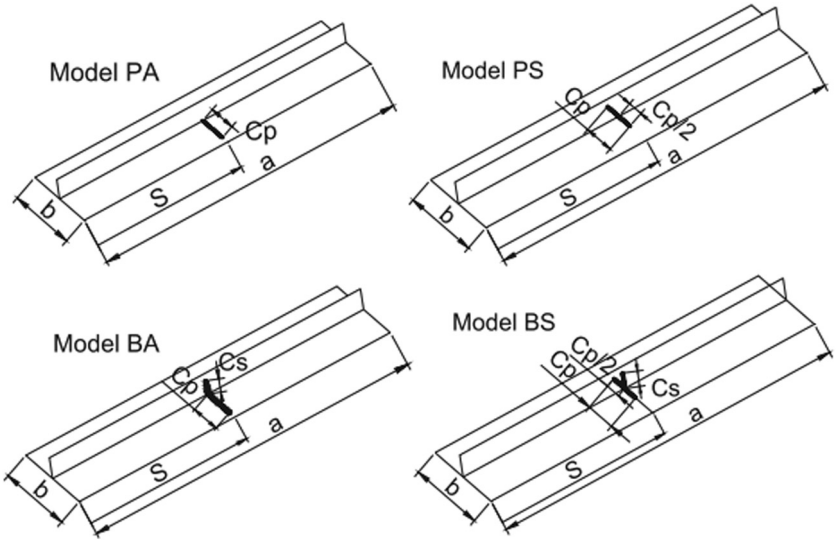

Figure 30: Four types of cracked models [77].

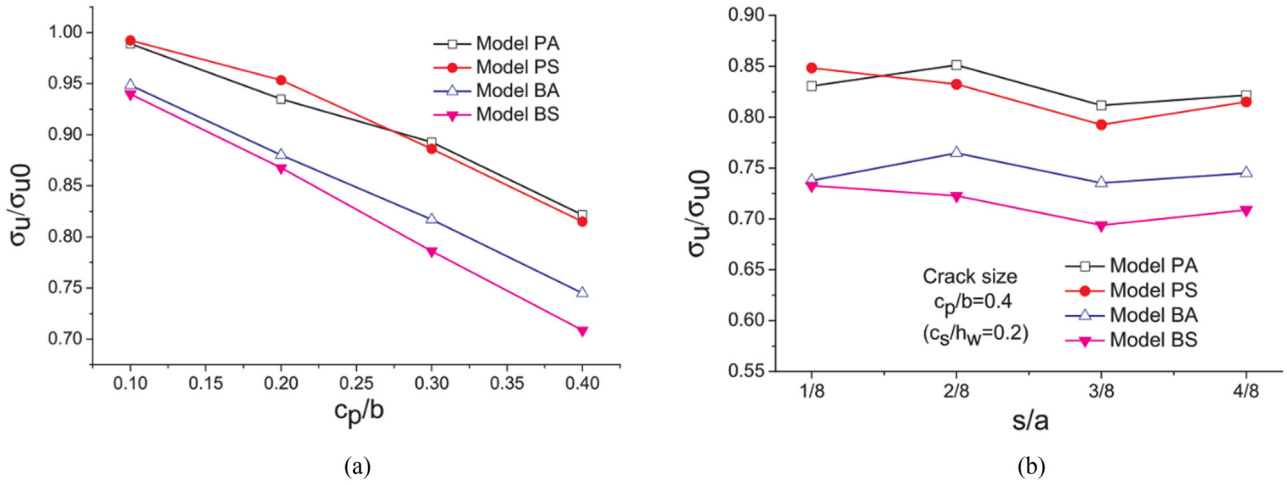

Figure 31: The ultimate compressive strength reduction characteristics of cracked stiffened plates as a function of (a) crack length and (b) longitudinal location of crack [77].

symmetric cracks in the plate-only case (PA *vs* PS) has a slight difference. In another case, variations in symmetric and asymmetric cases with crack locations in both the plate and stiffener result in a more significant gap as crack length increases. Meanwhile, in Figure 31(b), longitudinal crack locations do not appear to have a considerable effect on ultimate strength.

3.6 Various approach on applied modeling parameter through numerical analysis

In the analysis of stiffened panels using the numerical method, the selection of model configuration and boundary conditions is a crucial step that can significantly impact the analysis outcomes. Numerous studies have explored various variations of model configuration. Some examples discussed include the model configuration of ½ + ½ bay – ½ + ½ span, which was utilized in studies by Anyfantis [55] and Hanif *et al.* [56], as well as the ½ + 1 + ½ bay – ½ + 1 + ½ span configuration employed by Yu *et al.* [78]. In another parameter, the various definitions and approaches of boundary condition are also shown in several cases. In 2023, Lutfi *et al.*'s study [79] demonstrates the use of coupling conditions at the edges of the entire stiffened panel to provide specific degrees of freedom for deformation and rotation in accordance with the actual conditions. In his analysis of OTEC seawater tank stiffened panels, imposed displacements were also applied from two opposing directions, while nodes at the center of the plate were subjected to fixed constraint conditions.

In the different case, the research conducted by Xu *et al.* [14] compared the use of symmetric and periodic boundary conditions concerning ultimate strength and postbuckling behavior of stiffened panels. In this analysis, a stiffened panel with a Tee-bar configuration was selected, with material properties including a yield stress, Young's modulus, and Poisson's ratio of 313.6 MPa, 205.8 GPa, and 0.3, respectively. Two different configuration models were considered in the analysis: the ½ + 1 + ½ span and the ½ + ½ span. Variations were applied to the number of half-wave critical modes in initial imperfection, as presented in Table 7. The results obtained under periodic boundary conditions showed significant differences compared to symmetric boundary conditions when the buckling half-wave number was even. Conversely, in cases where the number of half-waves was odd, the results between the two boundary conditions were relatively similar due to the symmetry exhibited in the initial imperfection modes. The results from periodic boundary conditions did not overestimate the ultimate strength in various cases, whereas symmetric boundary conditions could only be applied when the collapse mode exhibited a symmetric shape. Therefore, the

Table 7: Number of half wave (m) in initial deflection in the longitudinal direction [14]

Boundary condition	Plate: a × b (mm)	P_x/P_y			
		1:0	1:0.41	1:0.67	0:1
BC 1	2,550 × 850	3	1	1	1
	3,400 × 850	5	1	1	1
	2,890 × 850	3,4,5	—	—	—
BC 2	2,550 × 850	3	1	1	1
	3,400 × 850	5	1	1	1
	2,890 × 850	3,4,5	—	—	—

selection of boundary conditions should be made carefully to align with the structural characteristics under analysis.

A similar study was also conducted by Hanif *et al.* [15] to compare model configurations, boundary conditions, and methods for modeling transverse stiffeners when analyzing the strength of stiffened panels. This study was a parametric investigation without cross-combining various variations. Apart from comparing the postbuckling behavior for each variation, modifications were implemented to assess the time efficiency during simulations using ANSYS APDL. The variations in model configurations included ½ + ½ bay – ½ + ½ span, ½ + 1 + ½ bay – ½ + 1 + ½ span, and ½ + 1 + 1 + ½ bay – ½ + 1 + 1 + ½ span. Regarding the modeling of transverse stiffeners, different approaches were employed, such as modeling them in 3D or applying boundary conditions as fixed constraints on the transverse stiffener. Geometric dimensions of transverse stiffeners were also adjusted based on the research conducted by Platypodis and Anyfantis [80]. The results obtained by modifying the model configurations showed a trend of increasing ultimate strength values as the scope of model configurations expanded. The largest difference in ultimate strength occurred in the smallest model configuration, with variations reaching up to approximately 37 MPa. As for the modeling of transverse stiffeners, differences were observed between 3D modeling and not including such modeling. However, these differences were relatively small, not exceeding 10 MPa, as observed in Figure 32. In addition, variations in geometric aspects of modeling transverse stiffeners did not exhibit significant differences, with the largest variation being less than 0.5 MPa. When comparing the time required for the analyses, significant differences were noted in the modeling of model configurations, as indicated by labels A1, A2, and A3 in Figure 33. In this figure, modeling the ½ + 1 + 1 ½ bay – ½ + 1 + 1 + ½ span configuration consumed 1,223 s in a single simulation, whereas the ½ + ½ bay – ½ + ½ span model only required 144 s, representing more than eight times less time consumption per computation.

As discussed earlier, stiffened panels play a crucial role in reinforcing ship structures during both hogging and sagging conditions. Analyses involving single loads, such as compression, and combinations of loads have been extensively conducted with advanced improvisations, including the introduction of initial imperfections like corrosion, residual stress, and both global and local imperfection modes. However, continuous development is essential to enhance the safety of ship structures through various methods, particularly numerical techniques that show promising potential in modeling different types of imperfections. All the studies mentioned earlier are summarized in Table 8.

3.7 Stiffened curved plate structure

After discussing various variations present in stiffened panels, particularly flat stiffened panels, there exists another type of stiffened panel that constitutes the hull girder structure of a ship. Stiffened curved panels are reinforcement structures commonly found in the deck area with a camber, as well as on the front and rear sides of the hull, as illustrated in Figure 34. In comparison to flat stiffened panels, curved stiffened panels have received less attention in research.

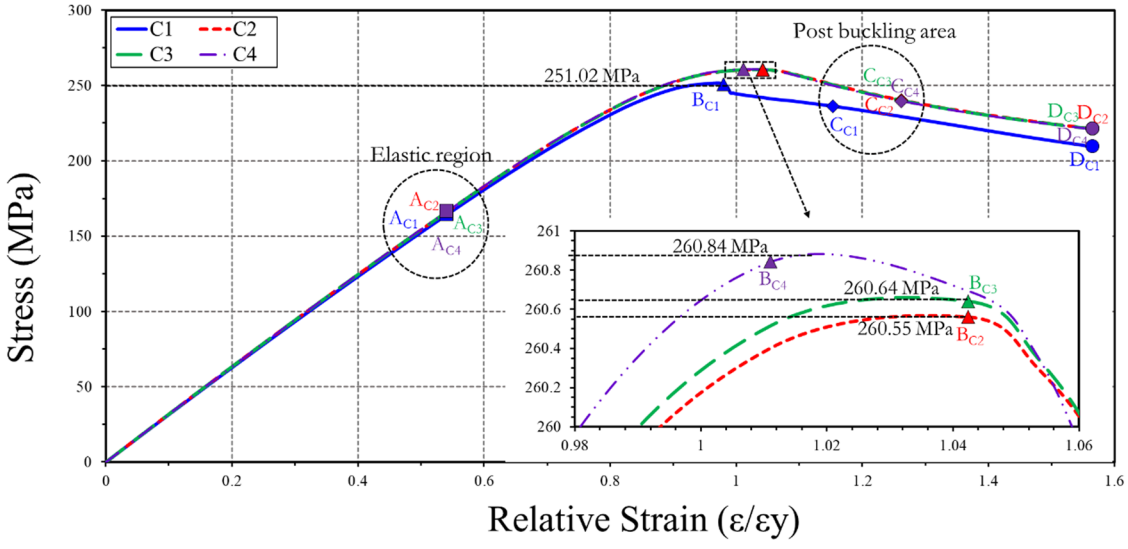

Figure 32: Stress–relative strain curves of related transverse stiffener modeling parameters [15].

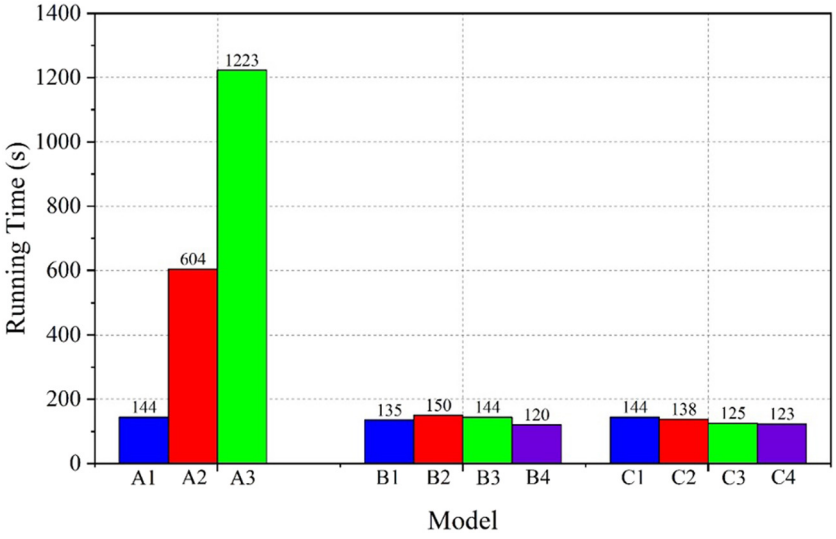

Figure 33: Running time consumed on each model [15].

Typically, research efforts have been confined to curved plates. An example is the investigation conducted by Maeno *et al.* [81], which focused on unstiffened curved plates to understand buckling and collapse behavior under axial compression. Similar investigations were also carried out by Yumura *et al.* [82], varying the curvature of the plate. Kwen *et al.* [83] undertook more diverse modifications involving aspect ratio, slenderness ratio, curvature, and various loading conditions, including longitudinal compression, transverse compression, and shear loads.

In the analysis of curved stiffened panels, different approaches are employed, such as numerical analysis [85] and empirical formulas [86]. Park *et al.* [87] conducted an analysis on curved stiffened panels by modifying the type of stiffener, curvature, flank angle, and plate slenderness ratio. Three different types of stiffeners, namely, flat, angle, and tee bars, were utilized in their study. The container ship type with a range of ½ + ½ bay – ½ + ½ span range was subjected to simply supported conditions on all sides except the loading edge. The scope of the model range area and the imposition of boundary conditions can be observed in Figure 35.

In addition to the aforementioned variations, geometric modifications were made to web height, web and flange thickness, and plate thickness, with respective variations of 50–400, 12–15, and 12–26 mm, respectively. The plate width varied between 1,000 and 3,000 mm, and the flank angle ranged from 50 to 450. Apart from geometric variations, Park *et al.* [87] also considered the influence of initial deflection, such as plate and web imperfection buckling modes. The research results on curvature and stiffener height variations indicated a proportional relationship between the increase in flank angle and web height with respect to ultimate strength.

Similar research was also conducted by Seo *et al.* [86], varying the values of curvature, plate slenderness ratio, web height, and three types of stiffeners. At a glance, the study conducted by Seo *et al.* [86] appears simpler as it involves fewer geometric parameters and is subjected to only one type of loading, namely, axial compression. However, toward the conclusion of their investigation, Seo *et al.* [86] were able to formulate an empirical calculation formula for determining the ultimate strength of curved stiffened panels. The influence of initial imperfection in the form of plate and torsional imperfection buckling modes was also considered, with a singular value set at 25% or slight level.

Numerical results indicated that the choice of stiffener type did not affect the ultimate strength values but did impact the collapse pattern. In the case of the flat bar, structural failure was attributed to the stiffener, while in the other two types of stiffeners, failure was caused by the plate and local stiffener. As mentioned earlier, the empirical formula for ultimate strength was derived by considering the plate slenderness ratio parameter and limiting the accuracy level of the results with the flank angle, as demonstrated in Eqs. (29) and (30).

$$\frac{\sigma_U}{\sigma_y} = \frac{1}{\sqrt{0.0683 + 0.994\beta' + 0.0065\beta'^2}}, \quad (\theta \le 5°), \tag{29}$$

$$\frac{\sigma_U}{\sigma_y} = \frac{1}{\sqrt{1.1339 - 0.1291\beta' - 0.0392\beta'^2}}, \quad (\theta > 5°). \tag{30}$$

Further development of stiffened panel structure strengthening endeavors has risen and demonstrated by Chen *et al.* [88].

Table 8: Milestone studies related to stiffened panel analysis

Test type	Material	Analysis method	Author	Title	Important remarks	Year
Compression	Steel	Experiment, numerical, and analytical	Lin [49]	Ship longitudinal strength modeling	Formulating a formula that takes into account not only plate slenderness but also column slenderness, the influence of initial imperfections, and residual stress	1985
Lateral load	ASTM A370	Experiment	Hu *et al.* [48]	Ultimate collapse tests of stiffened-plate ship structural units	The "damaged" specimen dimensions exhibit different and inconsistent behavior compared to the "undamaged" specimen	1997
Combination of axial compression and bending	Steel	Numeric	Grondin *et al.* [73]	Buckling of stiffened steel plates – a parametric study	The reduction in strength due to the effect of residual stress is significant because of the potential combination of residual stress and average buckling stress	1999
Four point bending	Steel	Experiment	Dexter and Pilarski [76]	Crack propagation in welded stiffened panels	The reduction in crack propagation rate is caused by the compressive residual stress effect between stiffeners	2002
Compression	Aluminum	Numeric	Rigo *et al.* [54]	Sensitivity analysis on ultimate strength of aluminum stiffened panels	The effect of reducing the yield stress in the HAZ by 10% results in a decrease in the ultimate strength value ranging from 2% to 5%	2003
Longitudinal stress	Composite	Composite column theory	Chen *et al.* [88]	Reliability analysis of a ship hull in composite material	The evaluation of ultimate longitudinal strength involves the utilization of equations derived from composite column theory. To assess structural integrity, a hybrid approach combining the response-surface method and the first-order reliability method is utilized to ascertain safety indices and the likelihood of failure	2003
Axial compression	HT32 steel	Numerical and analytical	Zhang and Khan [21]	Buckling and ultimate capability of plates and stiffened panels in axial compression	A semi-analytical formula for ultimate compressive strength assessments of stiffened panels was proposed applied to the deck and bottom structures for a range of various sizes oil tankers and bulk carriers for flat, L, and Tee bar type stiffened panel	2009
Compression	Steel	Numeric	Khan and Zhang [74]	Effects of welding-induced residual stress on ultimate strength of plates and stiffened panels	The load-end shortening curve without residual stress experiences a sharp drop after collapse, while in the case of a stiffened panel with residual stress, it tends to be smoother, and the "no-load shedding zone" increases	2011
Biaxial	High strength steel	Numeric	Gandhi *et al.* [62]	Ultimate strength analysis of stiffened plates with initial imperfections	Local and column imperfection modes with a single amplitude of 100% on Tee and Angle Bar type members provide a level of accuracy consistent with the ALPS – ULSAP and MSC MARC methods	2012

(Continued)

Table 8: *Continued*

Test type	Material	Analysis method	Author	Title	Important remarks	Year
Axial Compression	Steel	Experiment, numerical, and analytical through CSR	Xu and Soares [46]	Comparisons of calculations with experiments on the ultimate strength of wide stiffened panels	The results of the comparison between the three different numerical methods, experiments, and CSR on wide stiffened panels with the influence of initial imperfections showed that the CSR predicted the lowest ultimate strength	2013
Axial compression	Steel	Experiment	Xu and Soares [47]	Experimental study on the collapse strength of wide stiffened panels	The test configuration with a ½ + 1 + ½ bays model was able to avoid side bay collapse with simply supported boundary conditions and verified the use of FEM that aligns with it	2013a
Lateral displacement	S235JR-EN10025 and S255JR-EN10210	Experiment and numeric	AbuBakar and Dow [52]	Simulation of ship grounding damage using the FEM	Mesh density can affect the numerical result analysis	2013
Compression	No specified	Numeric	Xu *et al.* [14]	Influence of boundary conditions on the collapse behavior of stiffened panels under combined loads	Periodic boundary conditions do not overestimate the ultimate strength in various cases, while symmetric boundary conditions can only be applied when the collapse mode exhibits a symmetric form	2013
Compression	Steel	Numeric	Bayatfar *et al.* [75]	Residual ultimate strength of cracked steel unstiffened and stiffened plates under longitudinal compression	The effect of crack length significantly reduces the ultimate strength	2014
Axial compression	High tensile steel	Numeric and empirical formula	Seo *et al.* [86]	Nonlinear structural behavior and design formulae for calculating the ultimate strength of stiffened curved plates under axial compression	The numerical results indicate that the choice of stiffener type does not have an effect on the ultimate strength values but does influence the collapse pattern. In the case of the flat bar, structural failure is attributed to the stiffener, while in the other two types of stiffeners, failure is caused by the plate and local stiffener	2016
Compression	Steel Q345	Experiment	Zhang *et al.* [35]	Experimental analysis of residual ultimate strength of stiffened panels with pitting corrosion under compression	The variation in the location of pits and their diameter has an effect on strain distribution and results in a change in the buckling position	2017
Compression	Steel	Numeric	Feng *et al.* [65]	Reliability of the ultimate strength of ship stiffened panel subjected to random corrosion degradation	The random corrosion wastage of the stiffened panel on the bulk carrier mid-ship deck structures follows the log-normal distribution	2017
Compression	High tensile strength material	Numeric	Cui *et al.* [77]	Ultimate strength characteristics of cracked stiffened plates subjected to uniaxial compression	Variations in symmetric and asymmetric cases regarding the location of cracks in the plate and stiffener result in a larger gap as the crack length increases	2017

(Continued)

Table 8: *Continued*

Test type	Material	Analysis method	Author	Title	Important remarks	Year
Compression	Steel Q345	Experiment and numeric	Shi *et al.* [53]	Numerical assessment of experiments on the ultimate strength of stiffened panels with pitting corrosion under compression	The influence of pit corrosion, in general, reduces the ultimate strength value by up to 20.7%	2018
Combine loading (shear and compression)	Steel	Numeric	Rizzo and Caire [63]	Ultimate strength formulations for FPSO stiffened panels under combined compression and shear with initial imperfections and damage	The magnitude of the initial imperfection reduces the ultimate strength, and the reduction in ultimate strength is more sensitive to compression than to shear load	2018
Compression	Steel AH36	Experiment and numeric	Yu *et al.* [78]	Experimental and numerical investigation on the ultimate strength of stiffened plates with scanned initial geometrical imperfection	Stiffened panels measured using 3D scanning technology can be applied in the ultimate strength assessment	2019
Uniform and nonuniform compression	Steel	Numeric and analytic	Anyfantis [55]	Ultimate strength of stiffened panels subjected to nonuniform thrust	Simplify formula by the influence of initial imperfection and non-uniform thrust	2020
Compression	HT32 steel	Numeric	Feng *et al.* [64]	A parametric study on effects of pitting corrosion on stiffened panels' ultimate strength	Increasing the rate of DOP is correlated with a significant decrease in ultimate strength, and this effect intensifies as the pit depth increases	2020
Axial compression	High tensile steel	Numeric	Park *et al.* [87]	Estimation of buckling and ultimate collapse behavior of stiffened curved plates under compressive load	The research findings on variations in curvature and stiffener height indicate a proportional relationship between the increase in flank angle and web height with respect to ultimate strength	2020
Compression	No specified	Numeric	Georgiadis *et al.* [61]	Influence of stochastic geometric imperfection on the ultimate strength of stiffened panel in compression	The stochastic geometric imperfection model is capable of determining the imperfection model based on the maximum distortion magnitude and combining the effects of both	2021
Compression	Steel	Numeric	Li *et al.* [67]	The influence of residual stress on the ultimate strength of longitudinally compressed stiffened panels	When applied only to the local plate, residual stress reduces the ultimate strength by an average of about 6%. However, when applied to a combination of plate and web, it ranges around 8.5%	2021
Compression	No specified	Numeric	Li *et al.* [59]	A comparison of geometric imperfection models for collapse analysis of ship-type stiffened plated grillages	Different geometric imperfection models lead to an appreciable uncertainty in the ultimate compressive strength	2022
Compression	High strength steel	Numeric	Hanif *et al.* [15]	Effect of design parameters on the ultimate strength and collapse behavior of stiffened panels	The variation in the ultimate strength value resulted from differences in the range configuration model, boundary conditions, and transverse stiffener modeling was relatively negligible, indicating the overall appropriateness of the variations	2023

(Continued)

Table 8: *Continued*

Test type	Material	Analysis method	Author	Title	Important remarks	Year
Compression	High strength steel	Numerical and analytical	Hanif *et al.* [51]	Assessment of the ultimate strength of stiffened panels of ships considering uncertainties in geometrical aspects: Finite element approach and simplified formula	Proposes a simplified formula under variations of initial geometric imperfections in three imperfection modes, including column, torsional, and local imperfection modes, with variations in the slenderness and span-to-bay ratio	2023
Compression	High strength steel	Numeric	Hanif *et al.* [56]	Effects of the geometrical imperfections on the ultimate strength performances: A case study on the designed-steel stiffened panel	The initial geometric imperfection significantly reduces the ultimate strength and the prediction of ultimate strength according to IACS falls within the ultimate strength range with severity levels ranging from 25 to 100%	2023c
Lateral and transverse pressure	Steel	Numeric	Lutfi *et al.* [79]	Assessment of the stiffened panel performance in the OTEC seawater tank design: Parametric study and sensitivity analysis	The application of a transverse pressure of 0.16 MPa results in the largest reduction in ultimate strength for a stiffened panel with a plate aspect ratio of 6, which is approximately 7%	2023

Their study primarily delves into the calculation methodology for ultimate longitudinal strength and the reliability assessment of stiffened panel structures. Chen *et al.*'s work utilizes composite materials with a Young's modulus of 15 MPa in the panel sections. The assessment of ultimate longitudinal strength is conducted through equations derived from composite column theory. To evaluate structural integrity, a combination of the response-surface method and first-order reliability method is employed to determine safety indices and the probability of failure.

In a parallel investigation, Slater [89] directed his focus toward the integration of composites into stiffened panels, with particular consideration given to blast resistance. Slater's study utilizes GRP materials with the primary objectives of mitigating fatigue cracking, reducing overall weight, and enhancing fire resistance capabilities within the stiffened panels. This dual research effort contributes significantly to advancing the understanding and application of composite materials in shipbuilding, facilitating the development of lighter, stronger, and more resilient marine structures.

4 Box girder

A box girder is a structural component of a ship shaped like a hollow rectangle or box, which serves to provide strength to the ship's structure, consisting of plates, stiffeners, and transverse frames [90]. As a crucial structural element in a ship, the strength of the box girder is a highly critical subject in ship structure research. Therefore, intensive work has been conducted to analyze the behavior of ship structures with box girder specimens subjected to loads until reaching the ultimate strength limit. Box girders of this type are also used in bridge structures, as reported by Dowling [91], who conducted tests on box girders loaded at their midsections. The test results showed that shear loads and shear lag effects did not significantly impact the ultimate strength reduction of the box girder.

Early research on box girders was conducted by Reckling [92], who performed collapse tests on seven box girder models. Ostapenko [93] conducted tests on three box girder models using bending, shear, and torque loads. Nishihara conducted tests on eight different box girder models representing various types of conventional ships such as tankers, bulk carriers, and container ships. Another study by Mansour and yang [94] involved experimental testing of two large-scale box girders representing different types of ships. This research was further extended with variations in loads, methods, analysis approaches, and initial conditions of the box girder, including factors like cracks and corrosion.

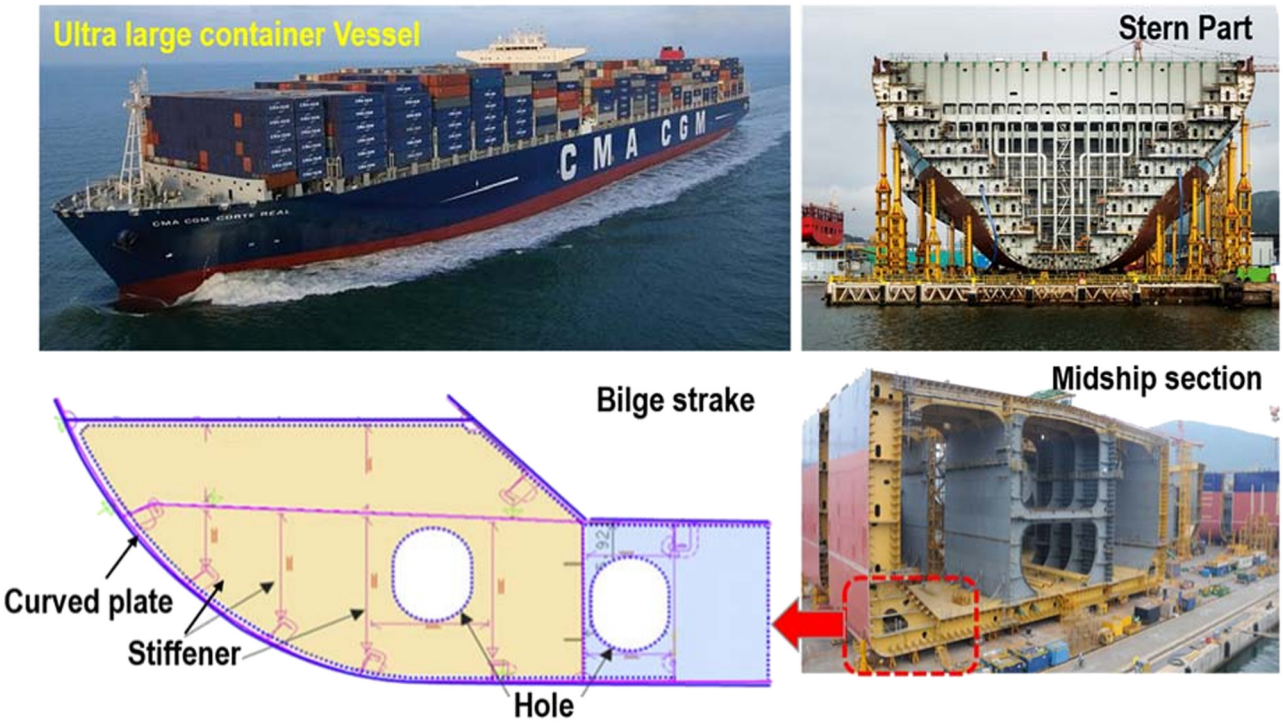

Figure 34: Cylindrically curved plate panel of ship structures [84].

4.1 Analysis of box girder

Experimental testing was conducted by Gordo and Soares [95], using pure bending tests on a box girder to induce collapse with compressive loads on the upper flange and tensile loads on the bottom part. Mild steel material with a yield stress of 240 MPa and Young's modulus of 210 GPa was used in this study. To obtain realistic values, tension tests were initially conducted to determine the average values. The experiments involved several loading cycles intended to release stress in the panel to very low levels. The resulting collapse is similar with the experiment conducted by Saad-Eldeen *et al.* [96] that can be observed in Figure 36.

Gordo and Soares [95] observed that the distribution of transverse strains at the center of the box girder indicated a decrease in the effectiveness of the reinforced panels under tension conditions, especially in areas far from the main vertical plates (web) and when subjected to significant moments. Strains detected in the middle of the panel were approximately half of what was observed at the corners. It is important to note that this strain pattern persisted even after the external load was removed. In addition, Gordo and Soares [95] stated that in panels subjected to compression, the strain distribution was less influenced by initial loading cycles, but significant plastic strains emerged during the collapse phase. The structural configuration after buckling matched the residual plastic strain distribution after collapse and load removal.

Experimental testing of box girders was conducted by Gordo and Soares [97] with the aim of determining the ultimate strength of box girders made from high-tensile steel, specifically HTS 690 material with yield stress and Young's modulus values of 690 MPa and 200 GPa, respectively. In this research, Gordo and Soares [97] applied a pure bending moment load to the box girder, with tension on the bottom part and compression on the upper part of the box girder. The box was made of 4 mm thick plates, and the spacing between longitudinal stiffeners was 150 mm at the top, as illustrated in Figure 37. Using the same experimental method as earlier, the experiments were conducted to apply multiple loading cycles aimed at obtaining stress relief in the panels. From this study, Gordo and Soares [97] stated that the efficiency of HTS 690 material was quite impressive when used in box girders subjected to bending moments. Intense rotational and axial deformations occurred in the middle frame, both on the upper and lower parts of the box girder. The ultimate bending moment obtained was 1,526 kNm.

Gordo and Soares [98] experimental research on box girders continued, focusing more specifically on box girders made of mild steel. Similar to the previous study, the box girders were tested using four loading cycles followed by unloading to identify and quantify the reduction in

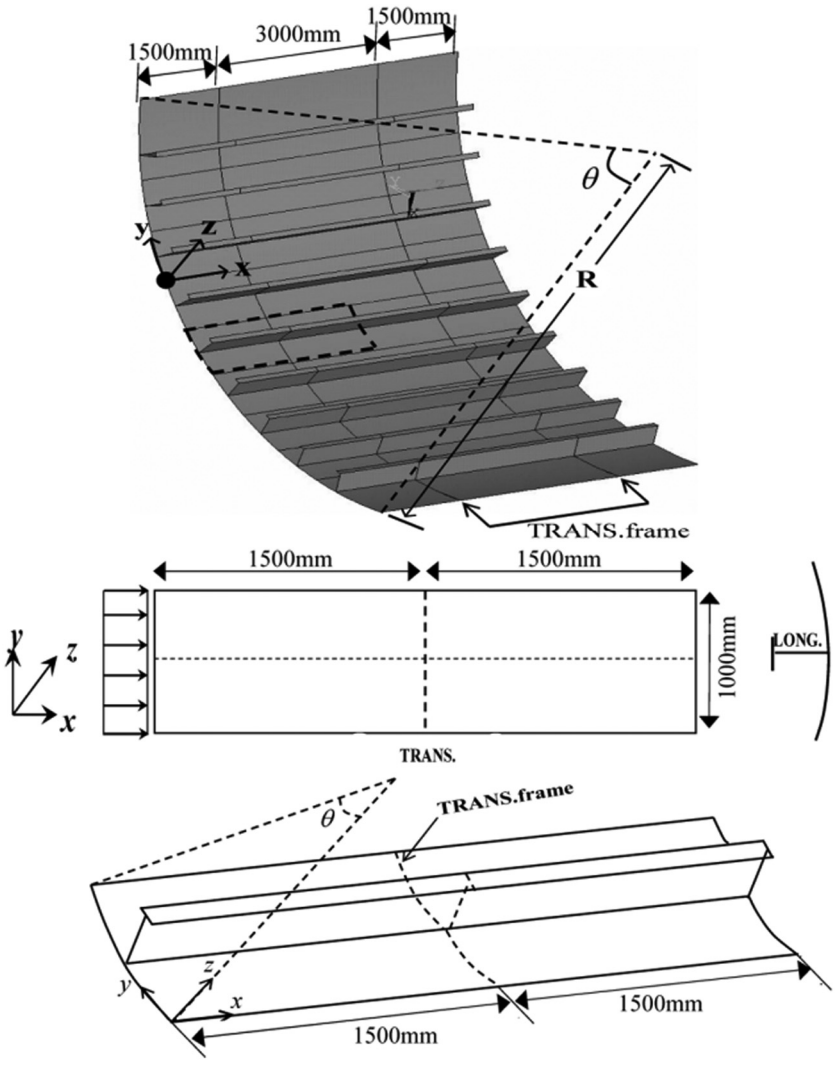

Figure 35: Double span/double bay model of stiffened curved plate [87].

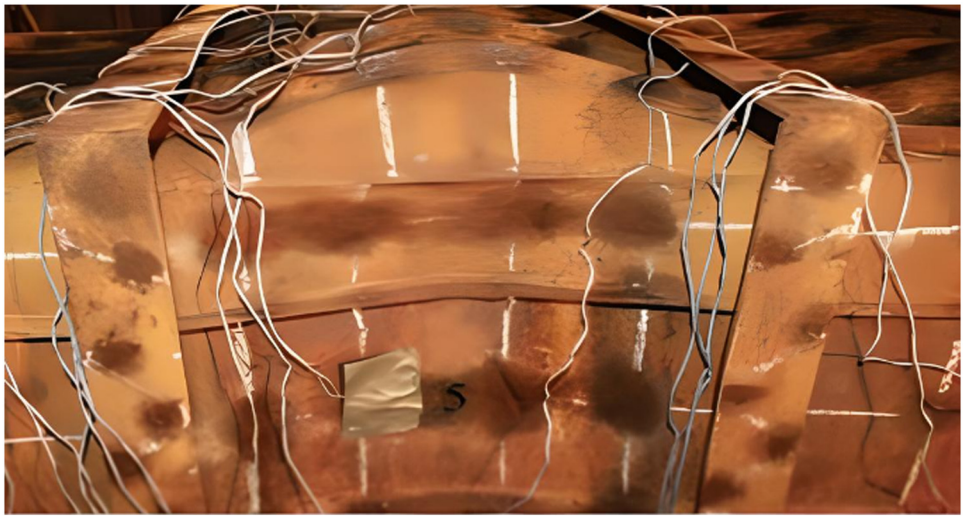

Figure 36: Permanent deformation occurs when structure collapse [96].

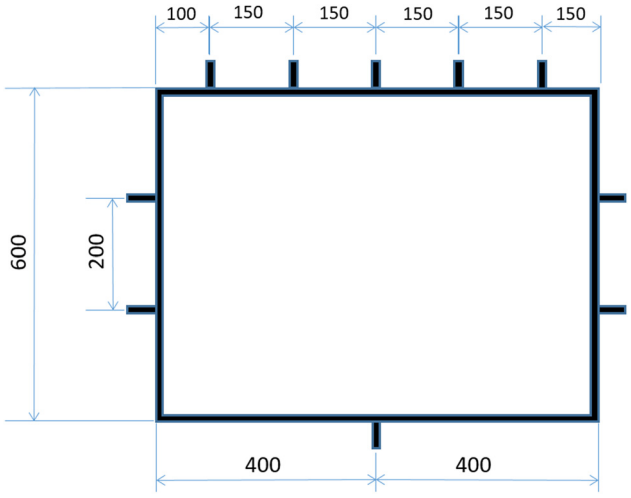

Figure 37: Geometry of Gordo and Soares' experiment redrawn [98].

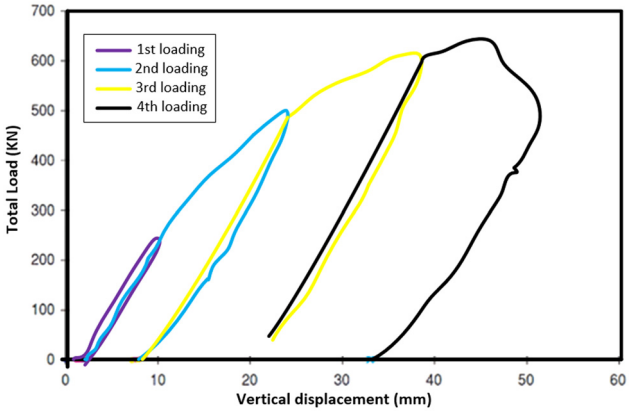

Figure 38: Graph of four loading cycles produced based on the information obtained from the study by Gordo and Soares [98].

residual stress resulting from welding. The results of the four loading cycles are shown in Figure 38.

Gordo and Soares [98] showed that the box girder performed as expected, with a maximum applied load of 643.0 kN and a resulting displacement of 45.3 mm. Gordo and Soares [98] emphasized that residual stresses were an important variable in this experiment and could influence the moment–curvature curves obtained. Furthermore, Gordo and Soares [98] concluded that column slenderness affected the type of structural failure, where a high column slenderness would lead to a sudden collapse, as seen in the experimental moment–curvature curves represented by shedding patterns.

In addition, Gordo and Soares [98] compared experiments conducted on mild steel box girders and high tensile steel box girders, noting differences in curvature, especially in vertical displacement. The energy dissipation in the early loading cycles of high-tensile steel box girders was considerably lower compared to that of mild steel specimens. Gordo attributed this difference to material properties related to the ductile behavior of the two materials.

In a study conducted by Shi *et al.* [99], the focus was on the dynamic response and ultimate strength of box girders subjected to bending moments. Shi *et al.* [99] used box girders with the same scantling section and span length as the experiments conducted by Paik [100] especially for MST-3 was selected as the object of analysis of that research. The main reason for the selection is the used model is convenient for showing the structural response difference between statics and dynamic bending moments. The model has a 540 mm span length, with 3.05 mm plating thickness, FB50 x 3.05 stiffener, and 180 mm stiffener spacing. The boundary conditions of the model used

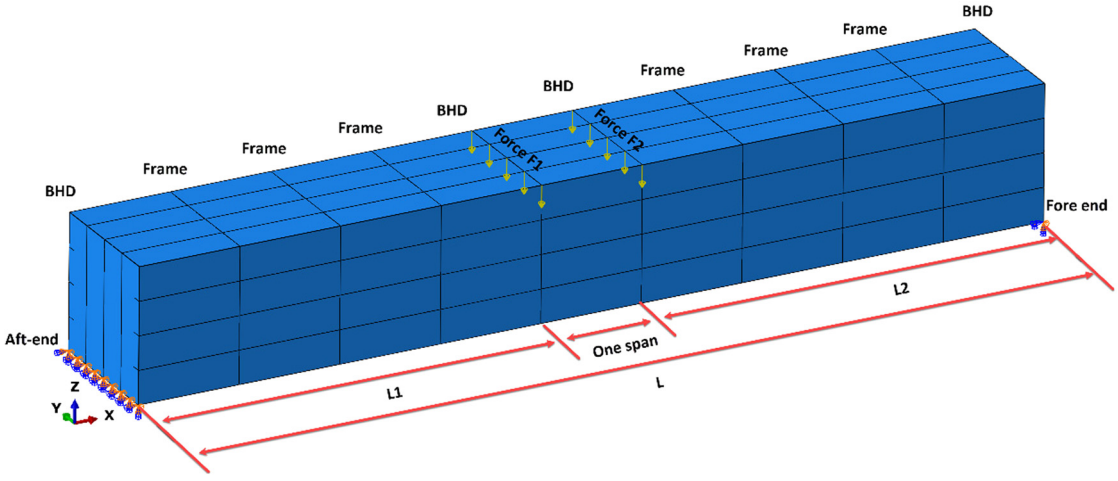

Figure 39: Boundary condition on Shi *et al.*'s research [99].

are shown in Figure 39. Using FEMs in Abaqus, Shi *et al.* [99] determined the dynamic ultimate bending moment and evaluation criteria. The study also considered the influence of model length, plate thickness, and loading duration.

In this study, it was concluded that under higher applied dynamic moments, the vibration period of the box girder increases due to local buckling and plastic deformation. In dynamic loading scenarios, several sections exhibit significant deformation simultaneously, unlike in static loading cases where usually only one section fails. In addition, Shi *et al.* [99] concluded that the length of the model has a significant influence on the dynamic ultimate moment when used for shorter durations. Longer models require a higher dynamic moment to reach a dynamic state.

4.2 Analysis of box girder with crack condition

Research on box girders with initial cracks was conducted by Shi and Wang [101]. In this study, box girders were subjected to torsional loads, and the analysis was performed using the FEM using the ABAQUS software. The various crack types considered in the study are illustrated in Figure 40. It was assumed that all cracks penetrate the thickness of the box girder, have no friction between their surfaces, and do not exhibit crack propagation.

Shi and Wang [101] conclude that when the ratio of crack length to cross-sectional width ($2c/b$) is less than 0.1, cracks will have a small effect on the ultimate strength of the box girder. However, a significant reduction in the ultimate strength of the box girder will occur when the ratio of crack length to cross-sectional width of the box girder is greater than 0.1. Shi and Wang [101] also stated that when the crack size is less than $2c/b = 0.3$, edge cracks will cause the greatest reduction in torsional ultimate strength. On the other hand, double-edge cracks will result in the highest reduction in torsional ultimate strength when $2c/b$ is greater than 0.3. Shi and Wang [101] formulated equations to predict the ultimate strength of cracked box girders, which have been verified with FEA.

In another study on box girders with cracks, the focus was on the variable of crack inclination in the box girder,

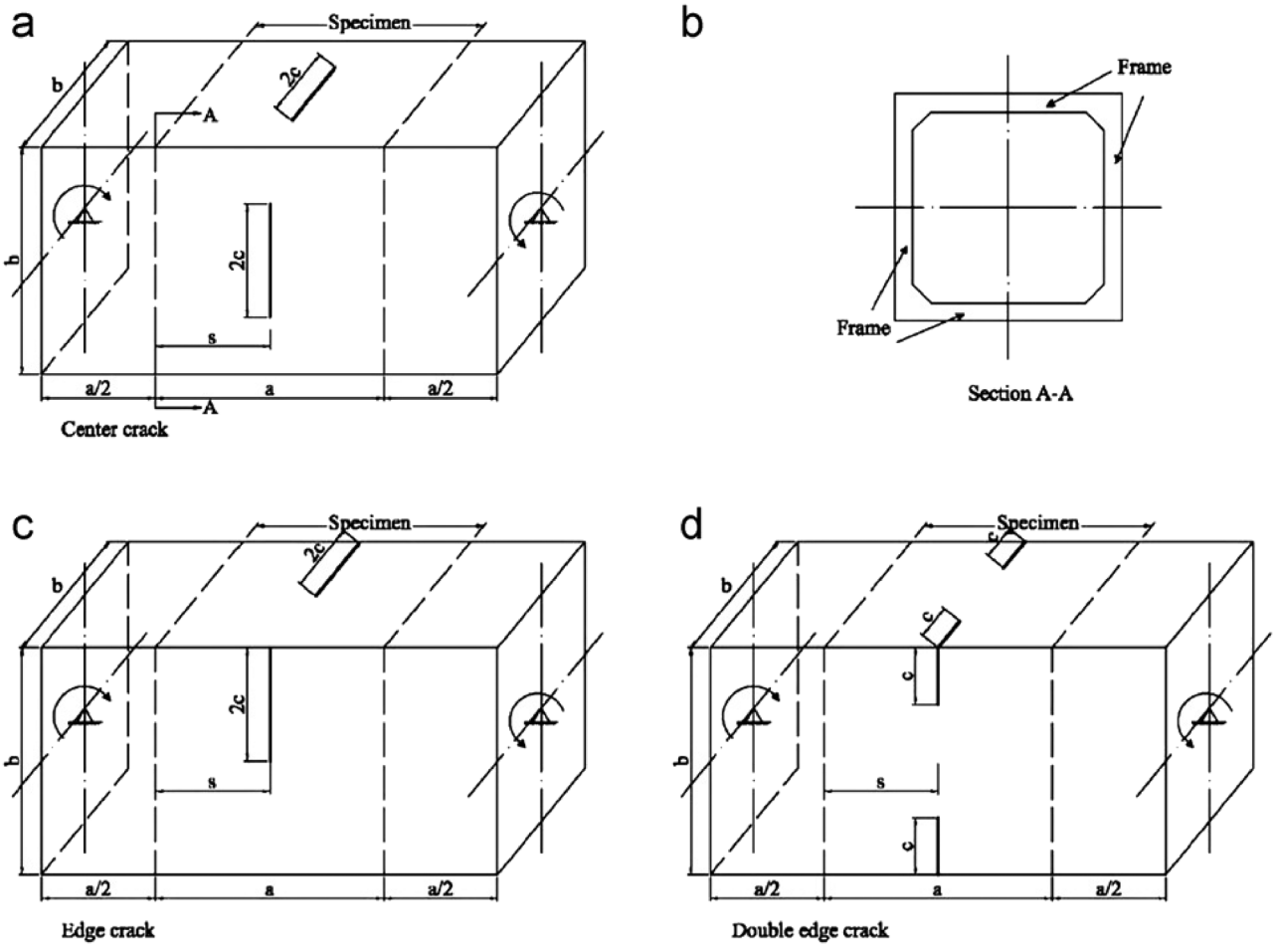

Figure 40: Crack type configuration; (a) Center crack, (b) Section A-A, (c) Edge crack, and (d) Double edge crack [101].

as conducted by Ao and Wang [102]. This research employed the FEM by ABAQUS with variations in crack inclination located in the middle of the box girder plate and subjected to torsional loads at both ends of the box girder. In addition, Ao and Wang [102] also considered crack size as a variable.

The results of Ao and Wang [102] research are shown in Figure 41. It can be seen that when the ratio of crack length to box girder section width (l/b) is less than 0.2, changes in the crack angle do not significantly impact the reduction in the ultimate strength of the box girder. However, a change in angle has a significant effect on ultimate strength when the ratio of crack length to box girder width exceeds 0.5. Ao and Wang [102] also stated that there is a linear relationship between ultimate strength and crack size, regardless of the angle variation. Meanwhile, there is a trigonometric relationship between ultimate strength and angle variation, especially when the ratio of crack length to box girder width is greater than 0.2.

Figure 42: Experimental setup on Saad-Eldeen *et al.*'s research [96].

4.3 Analysis of box girder with corrosion condition

Saad-Eldeen *et al.* [96,103] conducted a comprehensive study on corroded box girders. The initial research involved experiments on box girders subjected to four-point bending with a zero to initial corrosion condition, as depicted in Figure 42. In this study, it was found that the maximum vertical bending moment recorded on the test specimen was 580.55 kN, with a displacement of 28.57 mm. Subsequently, the results of this research are referred to as the "initial corroded box girder."

Saad-Eldeen *et al.* [104] conducted experimental testing on box girders with a focus on moderate corrosion levels. Furthermore, this research aimed to study the compressive failure strength of corroded box girders when subjected to four-point loading, resulting in a constant vertical bending moment. To induce corrosion, the box girder specimens were exposed to Baltic seawater without any corrosion protection. The water temperature and oxygen depolarization

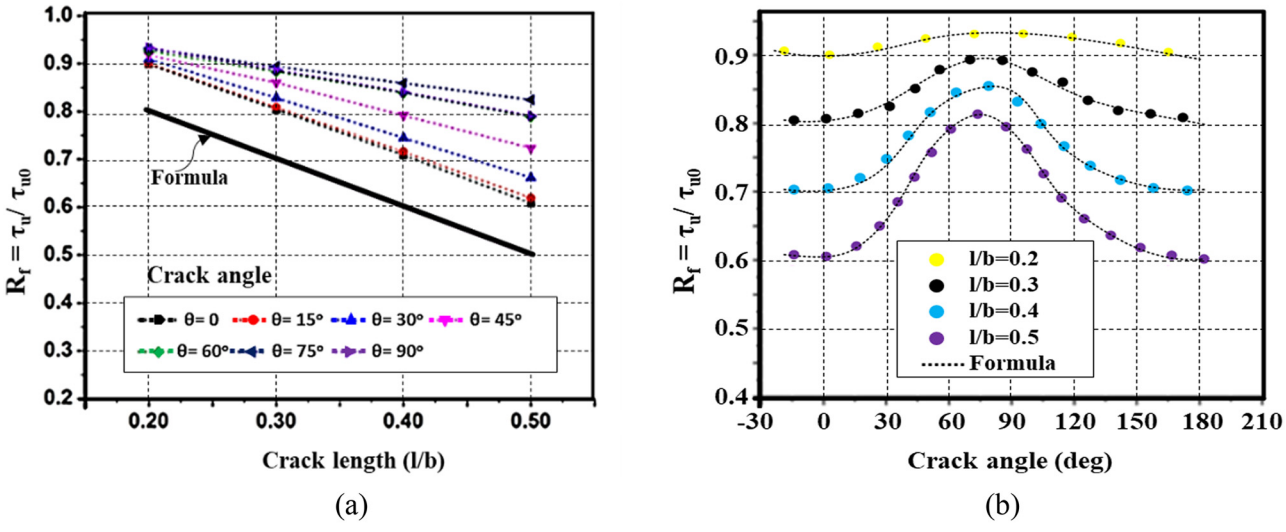

Figure 41: Relationship of ultimate strength and (a) crack length and (b) crack angle. Produced based on the information obtained from the study by Ao and Wang [102].

process were increased to accelerate the corrosion rate. This resulted in corrosion that reduced the weight of the box girder specimens by approximately 42 kg or 15% of their original weight. It was determined that the corrosion on the specimens was equivalent to 17.9 years of natural corrosion.

The testing was conducted in two loading cycles, where the first load was used to reduce residual stress, and the second load was the maximum load until collapse occurred in the box girder. Saad-Eldeen *et al.*'s [104] research findings indicated that the ultimate strength value of moderately corroded box girders decreased more significantly, by approximately 27.79%, compared to box girders that only experienced initial corrosion. The experimental results were also compared with existing equations, and Saad-Eldeen *et al.* [104] suggested that there should be consideration of the direct effect of corrosion on the mechanical properties of the material.

In a subsequent study, Saad-Eldeen *et al.* [105] conducted another assessment of the strength of severely corroded box girders. They used the FEM with nonlinear analysis and applied uniform vertical bending moment loads. Two corrosion degradation models were employed: one based on average general corrosion with thickness reduction and the other using thickness measurements at node locations in the finite element model. Initial imperfections in the finite element model were based on the initial imperfections by altering the vertical node positions

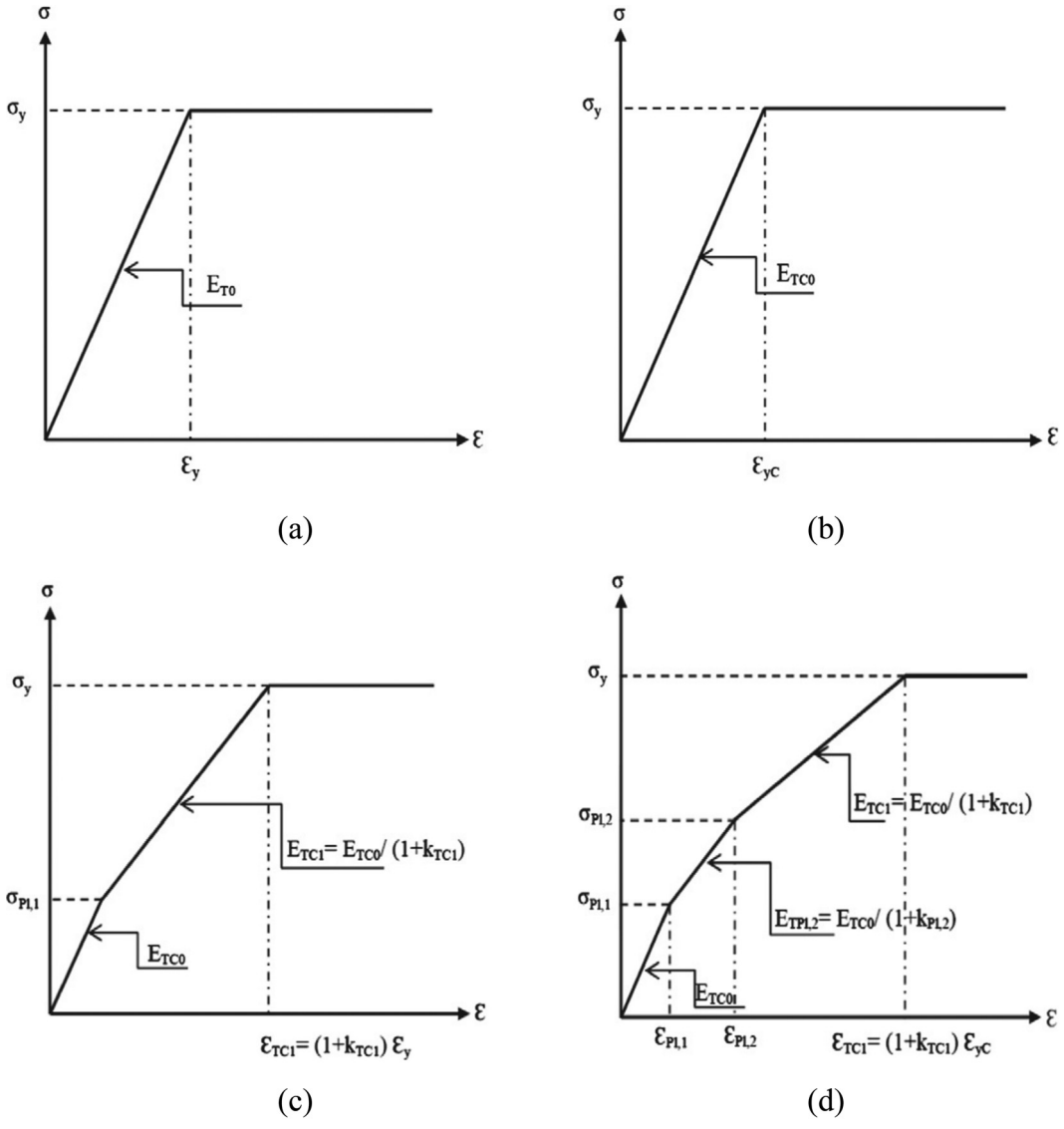

Figure 43: Existing stress–strain model [105]. (a) Elastic-plastic (EP), (b) elasto-plastic modified (EPM), (c) elasto-plastic modified 1 (EPM1), and (d) elasto-plastic modified 2 (EPM2).

in the finite element without affecting or adding stress to the specimen. The stress–strain relationship using existing equations and the experimental results from corroded box girders were also developed as shown in Figure 43.

The research results indicate a notable difference in ultimate bending behavior, ranging from 10 to 14.4%, between the outcomes obtained through FEA using the average corrosion thickness model and the real corrosion thickness model. This discrepancy underscores variations in the finite element model for deteriorated structures. In addition, among the available stress–strain models, Model EPM2 was proved to be a suitable stress–strain model for predicting curvature behavior and ultimate bending moment based on the available data from both the moment–curvature relationships in average corrosion and real corrosion scenarios.

Furthermore, in a subsequent experimental study, Saad-Eldeen *et al.* [90] compared the degrees of severity in box girders with initial corrosion, moderate corrosion, and severe corrosion. By cross-referencing with the corrosion data used in Saad-Eldeen *et al.*'s [96] research, it was determined that the box girder specimens used in this research were equivalent to 0.2 years of corrosion for initial corroded specimens, 17.9 years for moderately corroded specimens, and 23.3 years for severely corroded box girder specimens.

In the subsequent research conducted by Saad-Eldeen *et al.* [106], FEA was performed, and the results were compared with the experimental findings from their previous research. The same finite element model used in the previous study was employed. FEA was carried out, along with calculations using existing approaches and equations. The stress–strain relationship was developed by taking into account residual stresses and the effects of corrosion. Initial imperfections were added to the model, with respective depths of imperfection for the initially corroded, moderately corroded, and severely corroded cases being 1.72, 3.94, and 3.92 mm, respectively. Mechanical properties underwent degradation due to corrosion deterioration, particularly in the reduced value of the Young's modulus, which decreased by approximately 54.3%.

The results obtained using various stress–strain relationships, such as elastic–plastic and elastoplastic, considering hardening and weld toe effects, were compared with the ultimate bending moment results from experiments. It can be concluded that the results obtained from nonlinear finite element analysis with the utilized model are reasonably consistent with the experimental results, with differences or errors ranging from approximately 1–10% compared to the experimental results at each corrosion level. In addition, the comparison study was conducted with existing equations used in methods for calculating ultimate bending moments, as shown in Eqs. (31)–(35).

Faulkner and Sadden [107]:

$$M_{\mathrm{u}} = 1.15z\sigma_y\left[-0.1 + 1.4465 - 0.3465\left(\frac{\sigma_{\mathrm{u}}}{\sigma_{\mathrm{y}}}\right)^2\right], \tag{31}$$

Viiner [108]:

$$M_{\mathrm{u}} = \propto Z\ \sigma_{\mathrm{u}}, \tag{32}$$

Frieze and Lin [109]:

$$\frac{M_{\mathrm{u}}}{M_{\mathrm{p}}} = 0.172 + 1.548\frac{\sigma_{\mathrm{u}}}{\sigma_{\mathrm{y}}} - 0.368\left(\frac{\sigma_{\mathrm{u}}}{\sigma_{\mathrm{y}}}\right)^2. \tag{33}$$

Caldwell modified by Paik and Mansour [110]:

$$\begin{aligned} M_{\mathrm{u}} = {} & -A_{\mathrm{D}}(D-g)\sigma_{\mathrm{uD}} - A_{\mathrm{B}}g\sigma_{\mathrm{yB}} - A_{\mathrm{B}}'(g-D)\sigma_{\mathrm{yB}}' \\ & - \frac{A_S}{D}\left[(D-g)^2\sigma_{\mathrm{uS}} + g^2\sigma_{\mathrm{yS}}\right], \end{aligned} \tag{34}$$

Paik and Mansour [110]:

$$\begin{aligned} M_{\mathrm{u}} = {} & -A_D(D-g)\sigma_{\mathrm{uD}} - \frac{A_{\mathrm{S}}}{\mathrm{D}}(D-H)(D+H-2g_1)\sigma_{\mathrm{uS}} \\ & - A_{\mathrm{B}}g\sigma_{\mathrm{yB}} + \frac{A'_B}{H}(g_1 - D_{\mathrm{B}})[D_{\mathrm{B}}\sigma_{\mathrm{uS}} - (H-D_{\mathrm{B}})\sigma_{\mathrm{yS}}] \\ & - \frac{A_{\mathrm{s}}H}{3D}x[(2H-3g_1)\sigma_{\mathrm{uS}} - (H-3g_1)\sigma_{\mathrm{uS}}]. \end{aligned} \tag{35}$$

where A_{D}, A_{B}, A_{B}', and A_{S} are the total sectional area of the deck, outer bottom, inner bottom, and side shell, respectively; D is the hull depth; g is the neutral axis position above the baseline in the sagging condition; H is the depth of the hull section of the linear elastic state; σ_{uD} and σ_{uS} are the ultimate buckling strength for deck and side, respectively; σ_{yB}, σ_{yB}', and σ_{yS} are the yield strength of outer bottom, inner bottom, and side, respectively.

By using Eqs. 29–(33), the values of the ultimate bending moment for box girders under initially, moderately, and severely corroded conditions can be calculated and compared, as shown in Table 9. The highest error is evaluated at 33.4 and 33%, which are the comparisons between calculations using the Faulkner and Sadden [107] equation and experimental results for severely corroded box girders and experimental results with calculations using the Frieze and Lin equation [109] for moderately corroded box girders. The highest agreement is seen in the calculation using the Caldwell equation for initially corroded box girders, with an error of only 0.9%. It is also evident that the results of the analysis for the three types of box girders show an average change of 13.07%, with a 5.7% change in comparison between initially corroded, moderately corroded, and severely corroded box girders.

Tabel 9: Calculation result using existing formula and based on corrosion severity [106]

Ultimate bending moment	Initially corroded		Moderately corroded		Severely corroded	
	M_u	M_u (%)	M_u	M_u (%)	M_u	M_u(%)
Experimental result	568.9	—	382	—	201.1	—
Faulkner and sadden	687.5	20.8	382.6	0.16	268.1	33.4
Viner	558.2	1.9	305.8	20	213.7	6.3
Frieze and Lin	486.4	14.5	256.1	33	186.1	7.4
Caldwell modified, Paik and Mansour	563.7	0.9	268.9	29.6	199.1	0.9
Paik and Mansour	559.2	1.7	295.8	22.6	236.6	17.7

4.4 Analysis on box girder under combined crack and corrosion condition

Following previous separate studies on the strength analysis of corroded box girders with pit corrosion and cracks, Li *et al.* [111] conducted research by finite element analysis using the Abaqus software to analyze box girders subjected to vertical bending moments. Li *et al.* [111] also considered variables such as the bending mode, crack length, crack angle, and crack positions on both the plate and the position indicated on the cross-section of the specimen, and the diameter of pitting corrosion damage.

From this research, Li *et al.* [111] concluded that the variation in pitting corrosion diameter significantly affects ultimate strength. Similarly, as in the study of pitting corrosion, the total volume loss due to corrosion plays a significant role in the reduction of ultimate strength. It is also observed that the presence of bottom or side cracks has an impact on the reduction. For bottom cracks, the ultimate bending moment of the box girder in the hogging condition is much smaller than in the sagging condition. This is due to buckling that occurs at the bottom, enhanced by the presence of cracks. The influence of other crack parameters is then considered. It is evident that the projected length of transverse and inclined cracks and the actual length of longitudinal cracks located below the stiffener have a significant impact on the reduction in ultimate strength. However, longitudinal cracks have a smaller effect and almost no impact on the strength of the box girder.

Regarding cracks on the sides of the box girder, the reduction in ultimate strength in the sagging condition is much greater than in the hogging condition. When cracks are in vertical or inclined positions, the projected length of the cracks has a significant impact on the strength reduction of the box girder. When cracks shift toward the deck, the reduction becomes more significant. In general, it was shown that the reduction caused by either cracking or pitting corrosion is slightly larger than the reduction caused by coupled damage. However, the difference is too small so it could be neglected.

Further research has been conducted to ascertain the strength of other ship structures, such as box girders, through the application of composite materials, as evidenced by the study conducted by Soares *et al.* [112]. Soares *et al.* [112] conducted experimental and numerical investigations into the behavior of box girder structures using glass fiber-reinforced plastic (GFRP) materials. Specifically, the material employed was WR/polyester GRP. In the experimental phase, the study utilized four-point bending tests to assess the material strength of the structure. Meanwhile, numerical methods employed nonlinear finite element codes to predict the responses obtained from the box girder. The research revealed that the comparison between numerical results and experimental data demonstrated consistent findings, particularly regarding buckling moment, buckling mode, and the prebuckling and postbuckling behavior of the box girder structure.

As one of the structural components of a ship, the box girder also plays a significant role in the overall strength of the vessel. However, the diversity of research on box girders is relatively limited, indicating the need for further studies to advance ship structural development. A summary of the discussed research can be found in Table 10.

5 Conclusion

This article provides a comprehensive summary of research on ship structures, including plates, stiffened panels, and box girders. It encompasses various research methods, such as experiments, FEMs, and analytical calculation methods. The article also discusses the different loading conditions applied to the tested specimens. In addition, it considers the condition of ship structures, including initial states, corrosion, and the presence of cracks. Overall, the article demonstrates how these various testing conditions can significantly reduce the ultimate strength of ship structures.

Table 10: Milestone studies related to box girder analysis

Test type	Material	Analysis method	Author	Title	Important remarks	Year
Pure bending moment	Steel box	Experimental	Gordo and Soares [95]	Experimental evaluation of the ultimate bending moment of a box girder	The initial experiments on the box girder, which used bending moments, focused on residual stress and ultimate bending moment	1996
Four point bending	GFRP	Experiment and FEM	Soares *et al.* [112]	An experimental and numerical study on GFRP box girder under pure bending	Analysis conduct on GFRP material made box girder	2007
Pure bending moment	Mild steel box	Experimental	Gordo and Soares [97]	Experimental evaluation of the behavior of a mild steel box girder under bending moment	Experiments on mild steel box girder and its comparison with the ultimate strength of high tensile steel box girder	2008
Pure bending moment	High tensile steel	Experimental	Gordo and Soares [97]	Tests on ultimate strength of hull box girders made of high tensile steel J.M.	Experimental research on box girder with HTS 690 material, involving three different span variations	2009
Vertical bending moment load	Steel	Experimental	Saad-Eldeen *et al.* [103]	Experimental assessment of the ultimate strength of a box girder subjected to four-point bending moment	Vertical bending moment loading on a box girder	2010
Vertical bending moment load	Steel	Experimental	Saad-Eldeen *et al.* [96]	Compressive strength assessment of a moderately corroded box girder	Loading under moderate corrosion conditions on a box girder, equivalent to a ship that has been in service for 17.9 years	2011
Torsional loading	Steel	FEM	Shi and Wang [101]	Residual ultimate strength of cracked box girders under torsional loading	The finite element analysis used the software Abaqus, with the parameters of crack size and crack location. The ultimate strength reduction formula is also expressed as a function of these parameters	2012
Uniform bending moment	Steel	Experimental	Saad-Eldeen *et al.* [90]	Experimental assessment of corroded steel box-girders subjected to uniform bending	To compare the experimental results of three different severity levels of corrosion on box girders: initial, moderate, and severe	2013
Vertical Bending Moment	Steel	Experimental, FEM, numerical	Saad-Eldeen *et al.* [106]	Effect of corrosion severity on the ultimate strength of a steel box girder	To compare the results from numerical, experimental, and FEMs for three box girders with initial, moderate, and severe conditions	2013
Uniform vertical bending moment	Steel	FEM	Saad-Eldeen *et al.* [105]	Strength assessment of a severely corroded box girder subjected to bending moment	Two types of corrosion reduction were used: average general corrosion thickness reduction and the real thickness of the corroded plates	2014
Torsional load	Steel	FEM	Ao and Wang [102]	Ultimate strength of box girders with incline cracks	Finite element analysis of the box girder with crack conditions, followed by crack parameters	2015
Vertical	Steel	FEM	Li *et al.* [111]	Residual ultimate strength of stiffened box girder with coupled damage of pitting corrosion and a crack under vertical bending moment	In this study, an analysis is conducted on box girders under conditions of cracks, corrosion, and their combinations, along with various parameters	2021a
Bending moment	Steel	Experiment and FEM	Shi *et al.* [99]	Analysis of dynamic response and ultimate strength for box girder under bending moment	The analysis was conducted by also observing the dynamic response of the box girder using six models with variations in plate thickness and length	2023

Numerous investigations into ship plates and their load-testing capabilities have highlighted the considerable impact of several types of initial imperfections. These initial deflection and crack have been altered to include variations in angles, dimensions, and potential locations on ship plates. In addition, researchers have taken into account other factors, like pit corrosion, affecting one or both sides of the plate, aligning with the outcomes of corrosion-induced degradation. To gauge the unpredictability of these initial imperfections, Monte Carlo simulations were employed, enabling the assessment of the distribution of reductions in ultimate strength.

In the case of stiffened panels, research has been more diverse and comprehensive, encompassing experimental, analytical, and numerical studies. Variations in numerical methods have led to different approaches in model configurations, boundary conditions, and options for modeling transverse stiffeners in numerical analyses. Similar to ship plates, the introduction of initial imperfections influences the reduction in ultimate strength values. Moreover, different types of initial imperfections also affect the postbuckling behavior observed in stress–strain graphs, including the position of the ultimate strength and strain distribution differences. The development of numerical methods has provided variations in modeling, types, and magnitudes of buckling modes, cracks, and corrosion. In the realm of stiffened panel studies, numerical methods have been developed to extract data from random variations, allowing for the creation of analytical formulas that enhance the efficiency of predicting ultimate strength values.

Various studies have been conducted on box girders, with the majority focusing on modifications in geometry and materials. However, the influence of initial imperfections in box girders, specifically cracks and corrosion, remains relatively underexplored despite their prevalence in research on box girders under load. To date, the effects of initial deflection, as seen in ship plates and stiffened panels, have not been identified in the context of box girders. While there has been extensive research on plates and stiffened panels with numerous studies and data collection efforts as mentioned earlier, there is a notable gap in the number of studies and variations in parameters when it comes to ship box girder structures. To advance and enhance our knowledge of ship structures comprehensively, future research efforts should focus on conducting more comprehensive studies on ship box girder structures. This will help bridge the existing gap and contribute to a deeper understanding of ship structural integrity as a whole.

Acknowledgements: This work is part of the research activity conducted by Surabaya Merchant Marine Polytechnic in collaboration with the Research Center for Hydrodynamics Technology, National Research and Innovation Agency.

Funding information: Authors state no funding involved.

Author contributions: All authors have accepted responsibility for the entire content of this manuscript and consented to its submission to the journal, reviewed all the results and approved the final version of the manuscript. MIF: formal analysis, writing – original draft, writing – review and editing, visualization, project management. RA: conceptualization, methodology, formal analysis,writing – original draft, writing – review & editing, visualization.

Conflict of interest: Authors state no conflict of interest.

Data availability statement: The authors declare that the data supporting the findings of this study are available within the article.

References

[1] Zheng K. Analysis of the freight of handysize ships on the global bulk shipping market. The Maritime Commons: Digital Repository of the World Maritime University; 2018.

[2] Okubo M, Kuwahara T. Prospects for marine diesel engine emissioncontrol. New Technologies for Emission Control in Marine Diesel Engines. 1st edn. New York: Springer; 2020. p. 211–66.

[3] Prabowo AR, Sohn JM, Putranto T. Crashworthiness performance of stiffened bottom tank structure subjected to impact loading conditions: Ship-rock interaction. Curved Layer Struct. 2019;6(1):245–58.

[4] Prabowo AR, Sohn JM, Bae DM, Zakki AF, Harsritanto BI. Investigating crashworthy single and double skin structures against accidental ship-to-ship interaction. Curved Layer Struct. 2018;5(1):180–9.

[5] Fajri A, Prabowo AR, Muhayat N. Assessment of ship structure under fatigue loading: FE benchmarking and extended performance analysis. Curved Layer Struct. 2022;9(1):163–86.

[6] Mursid O, Tuswan T, Samuel S, Trimulyono A, Yudo H, Huda N, et al. Effect of pitting corrosion position to the strength of ship bottom plate in grounding incident. Curved Layer Struct. 2023;10(1):20220199.

[7] Prabowo AR, Sohn JM, Bae DM, Cho JH. Performance assessment on a variety of double side structure during collision interaction with other ship. Curved Layer Struct. 2017;4(1):255–71.

[8] Brubaker D. Marine pollution and international law: principles and practice. London: Belhaven Press; 1993.

[9] Wei C, Wang G, Cridland M, Olson DL, Liu S. Corrosion protection of ships. Handbook of Environmental Degradation of Materials. Norwich, New York: William Andrew Publishing; 2018. p. 533–57.

[10] Nwigwe T, Kiyokazu M. Statistical analysis of bulk carrier accident from 2011 to 2020. TransNav: Int J Mar Navig Saf Sea Transp. 2022;16:1.

[11] Du K, Monios J, Wang Y. Green port strategies in China. Green PortsInland and Seaside Sustainable Transportation Strategies. Cambridge, MA: Elsevier; 2019. p. 211–29.
[12] Kim DK, Lim HL, Kim MS, Hwang OJ, Park KS. An empirical formulation for predicting the ultimate strength of stiffened panels subjected to longitudinal compression. Ocean Eng. 2017;140:270–80.
[13] Xu MC, Song ZJ, Zhang BW, Pan J. Empirical formula for predicting ultimate strength of stiffened panel of ship structure under combined longitudinal compression and lateral loads. Ocean Eng. 2018;162:161–75.
[14] Xu MC, Yanagihara D, Fujikubo M, Soares CG. Influence of boundary conditions on the collapse behavior of stiffened panels under combined loads. Mar Struct. 2013;34:205–25.
[15] Hanif MI, Adiputra R, Prabowo AR, Muhayat N, Marta AS, Huda N, et al. Effect of design parameters on the ultimate strength and collapse behaviour of stiffened panels. J Appl Eng Sci. 2023;21(3):940–56.
[16] Adiputra R, Yoshikawa T, Erwandi E. Reliability-based assessment of ship hull girder ultimate strength. Curved Layer Struct. 2023;10(1):20220189.
[17] Denev Y. Corrosion waste impact on ship girder strength through life cycle. TransNav, Int J Mar Navig Saf od Sea Transp. 2024;18(2):415–8.
[18] Cui W, Wang Y, Pedersen PT. Strength of ship plates under combined loading. Mar Struct. 2002;15(1):75–97. doi: 10.1016/S0951-8339(01)00009-0.
[19] Guedes Soares C. Design equation for ship plate elements under uniaxial compression. J Constr Steel Res. 1992;22(2):99–114. doi: 10.1016/0143-974X(92)90010-C.
[20] Zhang S. A review and study on ultimate strength of steel plates and stiffened panels in axial compression. Ships Offshore Struct. 2016;11(1):81–91. doi: 10.1080/17445302.2014.992610.
[21] Zhang S, Khan I. Buckling and ultimate capability of plates and stiffened panels in axial compression. Mar Struct. 2009;22(4):791–808. doi: 10.1016/j.marstruc.2009.09.001.
[22] Box TA. Practical Treatise on the Strength of Materials. London: Spon; 1883.
[23] Karman Tv. Die mittragende Breite (The effective width). Berlin: Springer; 1924.
[24] Schnadel G. Proceedings 3rd International Congress on Applied Mechanics. 1930, Stockholm: 1930.
[25] Frankland JM. The strength of ship plating under edge compression. US EMM Report. Vol. 469; 1940.
[26] Faulkner D. A review of effective plating for the analysis of stiffened plating in bending and compression. J Ship Res. 1975;19(1):1–17.
[27] Paik JK, Pedersen PT. A simplified method for predicting ultimate compressive strength of ship panels. Int Shipbuild Prog. 1996;43(434):139–57.
[28] Paik JK, Kumar YVS, Lee JM. Ultimate strength of cracked plate elements under axial compression or tension. Thin-Walled Struct. 2005;43(2):237–72. doi: 10.1016/j.tws.2004.07.010]
[29] Paik JK. Residual ultimate strength of steel plates with longitudinal cracks under axial compression-experiments. Ocean Eng. 2008;35(17–18):1775–83. doi: 10.1016/j.oceaneng.2008.08.012.
[30] Paik JK. Residual ultimate strength of steel plates with longitudinal cracks under axial compression-Nonlinear finite element method investigations. Ocean Eng. 2009;36(3–4):266–76. doi: 10.1016/j.oceaneng.2008.12.001.
[31] Li D, Feng L, Xiao W. A study on residual ultimate strength of steel unstiffened plate with a crack. Appl Ocean Res. 2020;103(July):102336. doi: 10.1016/j.apor.2020.102336.
[32] Li D, Chen Z, Li J, Yi J. Ultimate strength assessment of ship hull plate with multiple cracks under axial compression using artificial neural networks. Ocean Eng. 2022;263(Sep):112438. doi: 10.1016/j.oceaneng.2022.112438.
[33] Zhang Y, Huang Y, Zhang Q, Liu G. Ultimate strength of hull structural plate with pitting corrosion damnification under combined loading. Ocean Eng. 2016;116:273–85. doi: 10.1016/j.oceaneng.2016.02.039.
[34] Silva JE, Garbatov Y, Guedes Soares C. Ultimate strength assessment of rectangular steel plates subjected to a random localised corrosion degradation. Eng Struct. 2013;52:295–305. doi: 10.1016/j.engstruct.2013.02.013.
[35] Zhang Y, Huang Y, Wei Y. Ultimate strength experiment of hull structural plate with pitting corrosion damage under uniaxial compression. Ocean Eng. 2017;130(Dec 2015):103–14. doi: 10.1016/j.oceaneng.2016.11.065.
[36] Ahmmad MM, Sumi Y. Strength and deformability of corroded steel plates under quasi-static tensile load. J Mar Sci Technol. 2010;15(1):1–15. doi: 10.1007/s00773-009-0066-1.
[37] Nakai T, Matsushita H, Yamamoto N. Effect of pitting corrosion on the ultimate strength of steel plates subjected to in-plane compression and bending. J Mar Sci Technol. 2006;11(1):52–64. doi: 10.1007/s00773-005-0203-4.
[38] Khedmati, MR, Nouri, ZHME, Roshanali MM. A comparative computational investigation on the effects of randomly distributed general corrosion on the post-buckling behaviour of uniaxially loaded plates. J Mech Sci Technol. 2012;26(3):767–83. doi: 10.1007/s12206-011-1222-1.
[39] Zhang J, Shi XH, Soares CG. Experimental analysis of residual ultimate strength of stiffened panels with pitting corrosion under compression. Eng Struct. 2017;152:70–86.
[40] Rahbar-Ranji A. Ultimate strength of corroded steel plates with irregular surfaces under in-plane compression. Ocean Eng. 2012;54:261–9. doi: 10.1016/j.oceaneng.2012.07.030.
[41] Fujita Y, Nomoto T, Niho O. Ultimate strength of stiffened plates subjected to compression. J Soc Nav Archit Jpn. 1977;141:190–7.
[42] Fujikubo M, Yao T, Khedmati MR. Estimation of Ultimate Strength of Ship Bottom Plating under Combined Transverse Thrust and Lateral Pressure. J Soc Nav Archit Jpn. 1999;186:621–30. doi: 10.2534/jjasnaoe1968.1999.186_621.
[43] Mouritz AP, Gellert E, Burchill P, Challis K. Review of advanced composite structures for naval ships and submarines. Compos Struct. 2001;53(1):21–42.
[44] Ma S, Mahfuz H. Finite element simulation of composite ship structures with fluid structure interaction. Ocean Eng. 2012;52:52–9.
[45] Mouhat O, Khamlichi A, Limam A. Reliability assessment of buckling for stiffened panels by considering localized geometric imperfections. Aust J Basic Appl Sci. 2013;7(8):616–24.
[46] Xu MC, Soares CG. Comparisons of calculations with experiments on the ultimate strength of wide stiffened panels. Mar Struct. 2013;31:82–101.
[47] Xu MC, Soares CG. Experimental study on the collapse strength of wide stiffened panels. Mar Struct. 2013;30:33–62.
[48] Hu SZ, Chen Q, Pegg N, Zimmerman TJ. Ultimate collapse tests of stiffened-plate ship structural units. Mar Struct. 1997;10(8–10):587–610.

[49] Lin YT. Ship longitudinal strength modelling. Doctoral dissertation. Ann Arbor, Michigan: ProQuest; 1985.
[50] Paik, JK, Thayamballi, AK. An empirical formulation for predicting the ultimate compressive strength of stiffened panels. ISOPE International Ocean and Polar Engineering Conference; 1997 May. ISOPE; 1997. p. ISOPE-I.
[51] Hanif MI, Adiputra R, Prabowo AR, Yamada Y, Firdaus N. Assessment of the ultimate strength of stiffened panels of ships considering uncertainties in geometrical aspects: Finite element approach and simplified formula. Ocean Eng. 2023;286:115522.
[52] AbuBakar A, Dow RS. Simulation of ship grounding damage using the finite element method. Int J Solids Struct. 2013;50(5):623–36.
[53] Shi XH, Zhang J, Soares CG. Numerical assessment of experiments on the ultimate strength of stiffened panels with pitting corrosion under compression. Thin-Walled Struct. 2018;133:52–70.
[54] Rigo P, Sarghiuta R, Estefen S, Lehmann E, Otelea SC, Pasqualino I, et al. Sensitivity analysis on ultimate strength of aluminum stiffened panels. Mar Struct. 2003;16(6):437–68.
[55] Anyfantis KN. Ultimate strength of stiffened panels subjected to non-uniform thrust. Int J Nav Archit Ocean Eng. 2020;12:325–42.
[56] Hanif MI, Adiputra R, Prabowo AR, Muhayat N, Erwandi E, Huda N. Effects of the geometrical imperfections on the ultimate strength performances: A case study on the designed-steel stiffened panel. Procedia Struct Integr. 2023;47:125–32.
[57] Fujikubo M, Yao T, Khedmati MR, Harada M, Yanagihara D. Estimation of ultimate strength of continuous stiffened panel under combined transverse thrust and lateral pressure Part 1: Continuous plate. Mar Struct. 2005;18(5–6):383–410.
[58] International Association of Classification Societies (IACS). Common Structural Rules for Bulk Carriers and Oil Tankers; 2022.
[59] Li S, Georgiadis DG, Samuelides MS. A comparison of geometric imperfection models for collapse analysis of ship-type stiffened plated grillages. Eng Struct. 2022;250:113480.
[60] Smith CS, Davidson PC, Chapman JC. Strength and stiffness of Ships'plating under in-plane compression and tension. R Inst Nav Archit Trans. 1988;130:1–20.
[61] Georgiadis DG, Samuelides MS, Li S, Kim DK, Benson S. Influence of stochastic geometric imperfection on the ultimate strength of stiffened panel in compression. Developments in the Analysis and Design of Marine Structures: Proceedings of the 8th International Conference on Marine Structures (MARSTRUCT 2021, 7-9 June 2021, Trondheim, Norway). Vol. 95; CRC Press; 2021.
[62] Gandhi PR, Doshi K, Vhanmane S. Ultimate strength analysis of stiffened plates with initial imperfections. Int J Innov Res Dev. 2012;1(10):190–206.
[63] Rizzo NA, Caire M. Ultimate strength formulations for FPSO stiffened panels under combined compression and shear with initial imperfections and damage. Lat Am J Solids Struct. 2018;15:e73.
[64] Feng L, Hu L, Chen X, Shi H. A parametric study on effects of pitting corrosion on stiffened panels' ultimate strength. Int J Nav Archit Ocean Eng. 2020;12:699–710.
[65] Feng GQ, Hu BN, Ren HL. Reliability of the ultimate strength of ship stiffened panel subjected to random corrosion degradation. China Ocean Eng. 2017;31:11–8.
[66] Wang G, Lee AK, Ivanov L, Lynch TJ, Serratella C, Basu R. A statistical investigation of time-variant hull girder strength of aging ships and coating life. Mar Struct. 2008;21(2–3):240–56.
[67] Li S, Kim DK, Benson S. The influence of residual stress on the ultimate strength of longitudinally compressed stiffened panels. Ocean Eng. 2021;231:108839.
[68] Smith CS, Anderson N. Strength of stiffened plating under combined compression and lateral pressure. Trans RINA. 1992;13(1):131–48.
[69] Yao T, Fujikubo M. Buckling and ultimate strength of ship and ship-like floating structures. Oxford: Butterworth-Heinemann; 2016.
[70] Paik JK, Thayamballi AK. Ultimate limit state design of steel-plated structures. Hoboken, New Jersey: John Wiley & Sons; 2003.
[71] Gordo JM, Soares G. Approximate load shortening curves for stiffened plates under uniaxial compression. Integr Offshore Struct. 1993;5:189–211.
[72] Yi MS, Hyun CM, Paik JK. An empirical formulation for predicting welding-induced biaxial compressive residual stresses on steel stiffened plate structures and its application to thermal plate buckling prevention. Ships Offshore Struct. 2019;14(Suppl 1):18–33.
[73] Grondin GY, Elwi AE, Cheng JJ. Buckling of stiffened steel plates – a parametric study. J Constr Steel Res. 1999;50(2): 151–75.
[74] Khan I, Zhang S. Effects of welding-induced residual stress on ultimate strength of plates and stiffened panels. Ships Offshore Struct. 2011;6(4):297–309.
[75] Bayatfar A, Khedmati MR, Rigo P. Residual ultimate strength of cracked steel unstiffened and stiffened plates under longitudinal compression. Thin-Walled Struct. 2014;84:378–92.
[76] Dexter RJ, Pilarski PJ. Crack propagation in welded stiffened panels. J Constr Steel Res. 2002;58(5–8):1081–1102.
[77] Cui C, Yang P, Li C, Xia T. Ultimate strength characteristics of cracked stiffened plates subjected to uniaxial compression. Thin-Walled Struct. 2017;113:27–38.
[78] Yu YZ, Feng GQ, Li CF, Ren HL. Experimental and numerical investigation on the ultimate strength of stiffened plates with scanned initial geometrical imperfection. China Ocean Eng. 2019;33:446–58.
[79] Lutfi YM, Adiputra R, Prabowo AR, Utsunomiya T, Erwandi E, Muhayat N. Assessment of the stiffened panel performance in the OTEC seawater tank design: Parametric study and sensitivity analysis. Theor Appl Mech Lett. 2023;13(4):100452.
[80] Platypodis EL, Anyfantis KN. On the modeling of ship stiffened panels subjected to uniform pressure loads. Appl Mech. 2022;3(1):125–43.
[81] Maeno Y, Yamaguchi H, Fujii Y, Yao T. Buckling/plastic collapse behaviour and strength of bilge circle and its contribution to ultimate longitudinal strength of ship's hull girder. In ISOPE International Ocean and Polar Engineering Conference. ISOPE; 2004.
[82] Yumura K, Katsura S, Ijima K, Yao T. Simulation of buckling collapse behaviour of cylindrically curved plates under axial compression. In Proceedings of TEAM Conference; 2005.
[83] Kwen YW, Park YI, Paik JK, Lee JM. Buckling and ultimate strength characteristics for ship curved plate structures. In Proceedings of the Annual Autumn Meeting. Sancheong Korea: SNAK; 2004. p. 351–6.
[84] Park JS, Paik JK, Seo JK. Numerical investigation and development of design formula for cylindrically curved plates on ships and offshore structures. Thin-Walled Struct. 2018;132:93–110.

[85] Oh YC, Kim KT, Ko JY. Investigation for Collapse Mode of Stiffened Curved Plate with Tee Shaped Stiffeners. J Korean Soc Mar Environ & Saf. 2011;17(3):295–300.
[86] Seo JK, Song CH, Park JS, Paik JK. Nonlinear structural behaviour and design formulae for calculating the ultimate strength of stiffened curved plates under axial compression. Thin-Walled Struct. 2016;107:1–17.
[87] Park JS, Ha YC, Seo JK. Estimation of buckling and ultimate collapse behaviour of stiffened curved plates under compressive load. J Ocean Eng Technol. 2020;34(1):37–45.
[88] Chen NZ, Sun HH, Soares CG. Reliability analysis of a ship hull in composite material. Composite Struct. 2003;62(1):59–66.
[89] Slater JE. Selection of a blast-resistant GRP composite panel design for naval ship structures. Mar Struct. 1994;7(2–5):417–40.
[90] Saad-Eldeen S, Garbatov Y, Guedes Soares C. Experimental assessment of corroded steel box-girders subjected to uniform bending. Ships Offshore Struct. 2013;8(6):653–62.
[91] Dowling PJ. Strength of steel box-girder bridges. J Struct Div. 1975;101(9):1929–46.
[92] Reckling KA. Behaviour of box girders under bending and shear. Proceeding of the ISSC. Paris, France; 1979. p. II–246.
[93] Ostapenko A. Strength of ship hull girders under moment, shear and torque. Proc. SSC-SNAME Symposium on Extreme Loads Response; 1981. p. 149–66.
[94] Mansour A, Yang JM, Thayamballi A. An experimental investigation of ship hull ultimate strength. SNAME. 1990;1(13):13–38.
[95] Gordo JM, Soares CG. Experimental evaluation of the ultimate bending moment. 1:1–14.
[96] Saad-Eldeen S, Garbatov Y, Soares CG. Experimental assessment of the ultimate strength of a box girder subjected to severe corrosion. Mar Struct. 2011;24(4):338–57.
[97] Gordo JM, Soares CG. Experimental evaluation of the behaviour of a mild steel box girder under bending moment. Ships Offshore Struct. 2008;3(4):347–58.
[98] Gordo JM, Soares CG. Tests on ultimate strength of hull box girders made of high tensile steel. Mar Struct. 2009;22(4):770–90.
[99] Shi GJ, Wang DY, Wang FH, Cai SJ. Analysis of dynamic response and ultimate strength for box girder under bending moment. J Mar Sci Eng. 2023;11(2):373.
[100] Paik JK. Ultimate limit state analysis and design of plated structures. Chichester, UK: John Wiley & Sons; 2018.
[101] Shi GJ, Wang DY. Residual ultimate strength of cracked box girders under torsional loading. Ocean Eng. 2012;43:102–12.
[102] Ao L, Wang D. Ultimate strength of box girders with incline cracks; 2015. p. 1–6.
[103] Saad-Eldeen S, Garbatov Y. Experimental assessment of the ultimate strength of a box girder subjected to four-point bending moment. 11th International Symposium on Practical Design of Ships and Other Floating Structures, PRADS 2010. Vol. 2; 2010. p. 1134–43.
[104] Saad-Eldeen S, Garbatov Y, Guedes Soares C. Compressive strength assessment of a moderately corroded box girder. Mar Syst & Ocean Technol. 2011;6(1):27–37.
[105] Saad-Eldeen S, Garbatov Y, Guedes Soares C. Strength assessment of a severely corroded box girder subjected to bending moment. J Constr Steel Res. 2014;92:90–102.
[106] Saad-Eldeen S, Garbatov Y, Guedes Soares C. Effect of corrosion severity on the ultimate strength of a steel box girder. Eng Struct. 2013;49:560–71.
[107] Faulkner D, Sadden JA. Toward a unified approach to ship structural safety. Trans RINA. 1979;121:1–28.
[108] Viner AC. Development of ship strength formulation. Proc. Int. Conf. on Advances in Marine Structures; 1986. p. 152–73.
[109] Frieze PA. Ship longitudinal strength modelling for reliability analysis. Proceedings of the Marine Structural Inspection, Maintenance, and Monitoring Symposium, SSC/SNAME. Arlington; Mar 1991. p. 18–9.
[110] Paik JK, Mansour AE. A simple formulation for predicting the ultimate strength of ships. J Mar Sci Technol. 1995; 1:52–62.
[111] Li D, Feng L, Huang D, Shi H, Wang S. Residual ultimate strength of stiffened box girder with coupled damage of pitting corrosion and a crack under vertical bending moment. Ocean Eng. 2021;235(July):109341.
[112] Soares CG, Chen NZ, Santos FM, Santos C. An experimental and numerical study on GFRP box girder under pure bending. Proceedings of MARSTRUCT'07, the 1st International Conference on Marine Structures. Glasgow, United KingdomAdvancements in Marine Structures. Paper: P2007-3 Proceedings; 2007.